

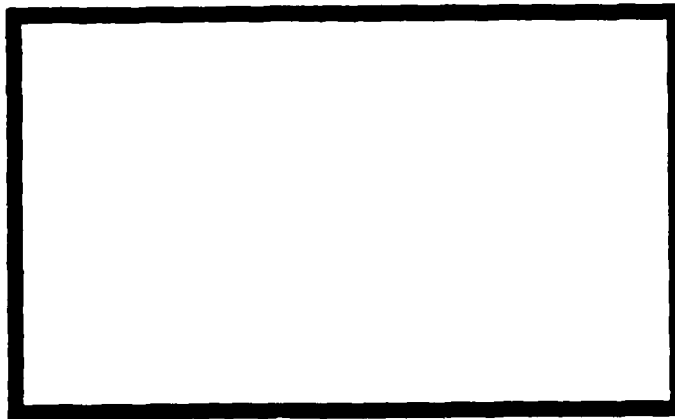
MICROCOPY RESOLUTION TEST CHART
NATIONAL BUREAU OF STANDARDS-1963-A

Final (10)



CAMBRIDGE UNIVERSITY

AD A111899



Engineering Department

DTIC FILE COPY

DTIC
EXTRACTED
MAR 11 1982
H

AFOSR-78-3644
Approved for public release;
distribution unlimited.

21

11

MICROMECHANISMS OF FRACTURE AND
HYGROTHERMAL AGING OF
FIBROUS COMPOSITES

P.W.R. Beaumont

CUED/C/MATS/TR.76 (1981)

U.S. AIR FORCE EUROPEAN OFFICE OF AEROSPACE (R & D)
London, England

AIR FORCE OFFICE OF SCIENTIFIC RESEARCH
Washington, D.C., U.S.A.

GRANT NUMBER AFOSR-78-3644

AIR FORCE OFFICE OF SCIENTIFIC RESEARCH (AFOSR)
NOTICE: This report is approved and is
distributed under the terms of AFOSR 190-12.
MATTHEW J. KEMNER
Chief, Technical Information Division

DTIC
SELECTED
MAR 11 1982
H

ABSTRACT

The micromechanisms of crack extension of carbon fibres, glass fibres, and hybrid composites containing glass fibres and carbon fibres in epoxy and polyester resins have been studied. A new collection of failure data has been summarized in cumulative probability diagrams and analysed using Weibull distribution parameters. This data, together with models of failure processes and information of work of fractures, is used to construct fracture-mechanism diagrams. These diagrams, together with the Weibull parameters may help in distinguishing between mechanisms of fracture; give guidance in selecting a material system; and in isolating aging and environmental effects.



Accession For	
NTIS	<input checked="" type="checkbox"/>
CRA&I	<input type="checkbox"/>
DTIC TAB	<input type="checkbox"/>
Unannounced	<input type="checkbox"/>
Justification	
By _____	
Distribution/ _____	
Availability Codes	
Dist	Avail and/or
	Special
A	

1. INTRODUCTION

In designing structural components from brittle materials, we assume that the operating stress does not exceed the strength of the material for an acceptable level of survival probability. Unfortunately, it is not so straightforward. The probability of failure will be affected by a variety of phenomena; for quasi-brittle fibrous composites, they include premature fracture of the fibres, and slow crack growth in the matrix and at fibre-matrix interfaces. The level of stress to initiate breakage of a fibre or failure of an interface depends upon the nature of the defect or flaw, its size and the way it interacts with the surrounding microstructure. For example, a weak fibre may fracture at a low stress but not propagate due to some localised plastic flow in the matrix. On the other hand, a small void at an interface or between two adjacent plies in a laminate may extend with ease along the length of the fibre. To complicate matters further, modes of failure are likely to be affected by environment and stress-state.

To have confidence in the design approach where working stress does not exceed ultimate strength for a permissible survival probability, therefore, requires information of the statistics of fracture and a detailed understanding of the micromechanisms of fracture of the material.

If a bar of quasi-brittle fibrous composite is pulled in tension, it may fail in one (or more) of several ways. It may, for example, fracture across the section and produce a flat surface analogous to cleavage fracture in metals. Alternately, it may fail by the propagation of a crack from one fracture plane to another producing a rough fibrous surface. If the composite is in the form of a laminate, it may fail by delamination and splitting, the precise mode of fracture and direction of crack growth depending upon the orientation of fibres and stacking geometry of the lamellae. At the microscopic level, fibres may debond, fracture at weak points below or on the fracture plane of the matrix, and pull-out. These micromechanisms of fracture occur in a zone surrounding the crack front which we call a microfracture damage zone. It is the work done in creating this damage zone which we equate to the toughness of the composite. The distance over which the fibre debonds and pulls out will depend on a number of intrinsic variables, fibre-matrix bond strength, distribution of flaws in the fibres, for example. A single composite, glass fibres in epoxy, for instance, can show all these modes of failure. It would be useful to have some idea of the

conditions under which each appears, the effect of intrinsic variables such as surface treatment of the fibre and ductility of matrix, and extrinsic variables, changes in temperature and humidity, for example.

This problem can be tackled in two complementary ways. The range of dominance of the more easily recognized mechanisms -- fibre pull-out, for instance -- can be determined by experiment. A change in temperature or humidity, or the passing of time in a given experiment, in which each mechanism appears can be noted.

Alternately, one might attempt to couple our understanding of the micromechanisms of cracking with models for each fracture process, and thereby predict the influence of bond strength or toughness of matrix on each mode of failure. To do so requires some way of quantifying fracture.

Models to describe the various micromechanisms of fracture in quasi-brittle fibrous composites have been described [1 - 5, for example].

This paper describes the statistical analysis of the micromechanisms of fracture of glass fibres and carbon fibres in polyester and epoxy, and mixtures of the two kinds of fibre in hybrid composites. Considerable failure data, based on the debonded and pulled out lengths of fibre, has been collected in fracture experiments and presented in cumulative probability diagrams.

A statistical analysis of the failure data is then carried out in order to obtain a characteristic value of the debonded and pulled out lengths of fibre for each fibre composite. Three mechanisms are briefly described by which these fibrous composites may fail, using a sequence in which they may occur. An equation is selected for each mechanism, based on a physically sound microscopic model, to describe each failure process in terms of the energy dissipated.

Each equation is then used, together with a value of fibre debond length and fibre pull-out length, to account for the fracture toughness of the composite, and dominant mechanism of toughening is apparent. Some of the work of fracture data in this paper are taken from previously published work [1,2].

The properties of the fibres and resins used in this study are listed in Table I.

2. FAILURE ANALYSIS OF FIBRE DEBOND LENGTH AND FIBRE PULL-OUT LENGTH

The procedure is as follows. We first assemble the available work of fracture data for the given material. We then tabulate a large amount of fractographic information on fibre-matrix debonding and fibre

TABLE I
Fiber and matrix properties

Material	No. of fibers per tow	Fiber diameter (10^{-6} m)	Tensile strength (GN m^{-2})	Young's modulus (GN m^{-2})	Failure strain ϵ
Carbon fiber Type II	5000	8	2.40	240	0.010
Glass Fiber Type E	1600	13	1.65	70	0.023
Typical Epoxy Resin	-	-	0.06	2.5	0.014
or Polyester Resin	-	-	-	-	-

pull-out processes. Each failure model is used in turn, together with the failure data to estimate the energy dissipated by the fracture mechanisms.

METHOD OF COLLECTING FAILURE DATA

There are (at least) two methods of collecting fractographic information. The first, and most common procedure, is to use a scanning electron microscope for observing fibres protruding above the fracture plane of the matrix. Several areas of the fracture surface are examined, photographs are taken and measurements of a few hundred pulled-out fibres are made. However, using this technique, nothing is learned about the fibre-matrix debonding process. A second technique involves the use of an optical microscope and the fracture of model fibrous composites. Such model composites can be in the form of a prismatic bar of transparent resin containing a single layer of unidirectional fibre tape and these have been described previously [1]. The beam is loaded in 3-point bending and the layer of fibres is subjected to a tensile stress (fig 1). Bundles of glass fibres and carbon fibres can be arranged in various ways to produce a series of composites ranging from a glass fibre composite to a carbon fibre composite, with many combinations between the two extremes. We can think of these model composites as single lamina from which is made the laminate (fig 2).

The area under the load/displacement curve is equated to the work to fracture the composite. Tracings are made of each debonded fibre region and each protruding bundle of fibres, observed in transmitted and reflected light, respectively, using an optical microscope (fig 3) [1].

Average values of the longest fibres extracted from a matrix and distances over which separation at the fibre-matrix interface have occurred are determined as follows. The area of each tracing is measured using a planimeter and is divided by the width of the fibre bundle. A summation of these values for each bundle is then made and divided by the total number of fibres in the bundles. For example, in specimens containing 5 strands of fibres, (where a strand contains 1,600 individual glass filaments or 5,000 individual carbon filaments), and where 20 tests have been carried out, 400 tracings are made of pulled out fibres and debonded fibres, since the two halves of each specimen can be viewed from both sides. Several hundred values of fibre debond length and fibre pull-out length can be made in this

way which are then tabulated. The technique was developed in this program and used throughout the study.

There are, of course, difficulties and ambiguities in a fractographic analysis of this sort. There is the assumption that the profile of the fibre debonded region does not change through the thickness of the bundle of fibres. Turning the test-piece over and examining from both sides will check this. We assume a normal distribution of pulled out lengths of fibre from zero, where the fibre breaks on the fracture plane of the matrix, and the maximum pull-out length, l_p . The average pull-out length is therefore $l_p/2$. We also assume that each fibre is extracted from its matrix socket without the attachment of fragments of resin onto the surface.

STATISTICAL ANALYSIS OF FAILURE DATA

The statistical predication of failure relies on the characterisation of a flaw strength distribution function [6]. One form of the extreme value distribution is

$$S = \exp \left(-\sigma/\sigma_0 \right)^m V \quad (1)$$

where S is the probability of survival, σ is an applied stress on a specimen of volume V , and m and σ_0 are the extreme value distribution parameters. The variability of a set of data decreases as m increases; m and σ_0 therefore characterise the material for prediction of structural reliability.

In logarithmic form, equation (1) can be written

$$\ln(-\ln S) = m(\ln \sigma - \ln \sigma_0) \quad (V = 1) \quad (2)$$

m is the gradient of a linear plot of $\ln(-\ln S)$ and $\ln \sigma$, and $\sigma = \sigma_0$ when $S = e^{-1} = 0.37$.

Each mechanism of failure in a fibre composite is affected by the statistical aspects of fibre-matrix bond strength, fibre strength, and the distribution of weak points along the length of fibre. This is why a broken fibre composite has a variability of lengths of pulled-out fibres protruding above the fracture surface. A quantitative assessment of failure therefore requires a statistical analysis of the micromechanisms of fracture; fibre pull-out length, for example, is likely to be affected by the distribution and strength of weak flaws along the length of the fibre. Equation (1) can be written in terms of the probability of a fibre debonding or pulling out over a

particular distance, l ,

$$P = 1 - \exp(-l/l_0)^m \quad (3)$$

where $P = 1 - S$.

The mean value, \bar{l} , of a distribution of data in the form of equation (3) can be expressed as

$$\bar{l} = \int_{l_1}^{l_n} (l \, dP/dl) \, dl \quad (4)$$

For the case of an extreme value distribution, the mean value, \bar{l} , can be expressed

$$\bar{l} = \int_{l_1}^{l_n} m(l/l_0)^m \exp(- (l/l_0)^m) \, dl \quad (5)$$

and \bar{l} determined from measured values of m and l_0 .

CUMULATIVE PROBABILITY DIAGRAMS SUMMARIZING FAILURE DATA

Cumulative probability diagrams can summarize a considerable amount of fractographic information on fibre-matrix debonding and fibre pull-out. They show a distribution of extreme values of fibre lengths and by presenting the data in logarithmic form, values of m and l_0 can be determined. These parameters, together with equation (5) are used to determine values of \bar{l} for fibre debonding and fibre pull-out.

Figure 4 shows cumulative probability versus fibre debond length, l_d , for model composites containing glass fibres in epoxy. The data does not overlap but are displaced slightly to higher values of l_d as the number of fibres increases. It seems that the debonding process is sensitive to the number of glass fibres in the resin. It is interesting to note, (although it is not obvious why), the data for $N = 4800$ fibres falls to the right of the data for $N = 6400$ fibres. This apparent reversal in trend in the shift of cumulative probability data will be referred to later when we discuss fracture energy. A similar shift of data towards higher fibre lengths is observed for pulled out glass fibres (fig 5). The apparent oddity in this case is the disproportionate displacement of data for $N = 8000$ fibres. Metallographic examination of various specimens showed excellent

penetration of the fibres with resin and the idea that poor wetting of the fibres is responsible for the movement of data to higher values is not correct.

The extreme value distribution equation can describe each set of data. The parameters m and l_0 are determined by replotting the data in logarithmic form, (fig 6). Presenting data in this way is useful for characterising modes of failure and for observing the subtle effects of environment, moisture for instance, on values of m and l_0 .

Combining equation 5 with values of m and l_0 enables us to determine the mean length of debonded and pulled out fibres. Table II lists values of m , l_0 and \bar{l} for the debonding and pulling out of glass fibres in epoxy. For comparison, values of the arithmetic mean of fibre debond length and fibre pull-out length are shown alongside \bar{l} calculated using equation 5.

Some glass fibre-epoxy specimens were stored at $18 (+2)^\circ\text{C}$, 65% R.H. for 6 months before testing. The distance over which the fibres debonded and pulled out are shown in cumulative probability diagrams (figs 7,8). Aging the composite has resulted in the data being displaced to lower values of debonding. The inference is that aging, (by whatever process), has increased the strength of the glass fibre-epoxy bond with a corresponding decrease in the distance over which the fibre debonds. It may be that additional curing and cross-linking of the resin with time is responsible for improvement in bonding, the effect of the matrix contracting around the fibres. If this is true, then an increase in bond strength, together with a decrease in fibre debond length would result in a fall in toughness of the composite. The measured work of fracture of glass fibre in epoxy is 280 kJ/m^2 , approximately, and 200 kJ/m^2 after storing for 6 months. In contrast, the pulling out of debonded glass fibres is unaffected by aging (fig 8). The distribution of values of pulled out fibres is dependent only on the flaw population of the fibre.

Fractographic information of glass fibres in a glass fibre/carbon fibre/ epoxy hybrid is summarized in the following cumulative probability diagrams (figs 9-11). The fibre debond length data do not superimpose, and increasing the ratio of glass fibres to carbon fibres may displace the data to the right or to the left of the diagram (fig 9). For example, increasing the glass fibre content from 30% (by vol.) to 56% (by vol.) of the total fibre content shifts the data from low values to high values; increasing the glass fibre content by a further 7%

TABLE II

A summary of m , ℓ_0 and $\bar{\ell}$ for glass fibres in epoxy

No. of glass fibre rovings	Fibre debond length (mm)		Fibre pull-out length (mm)	
	m	ℓ_0	$\bar{\ell}$ (arithmetic)	$\bar{\ell}$ (eq. 5)
1	3.1	2.3	1.7	2.0
2	3.6	2.7	2.4	2.5
3	3.1	3.6	3.2	3.2
4	3.5	3.3	3.0	3.0
5	4.6	4.2	3.8	3.9

Fibre pull-out length (mm)		Fibre pull-out length (mm)	
$\bar{\ell}$ (eq. 5)	$\bar{\ell}$ (arithmetic)	ℓ_0	m
0.09	0.12	0.12	1.5
0.10	0.11	0.11	2.0
0.13	0.14	0.14	1.9
0.13	0.15	0.15	1.9
0.22	0.25	0.25	2.2

(by vol.) moves the data back to lower values. Closer examination of the data shows the subtle effects of microstructure on the position of the cumulative probability curve. These effects will be referred to later.

In contrast, data of glass fibre pull-out length in the hybrid composite are almost superimposed (fig 10). The same applies to the data for carbon fibres (fig 11). Each cumulative probability curve overlaps one another and the shape and position of the curves are not significantly affected by variations in composition. The same data plotted in a logarithmic form, based on equation 6, is used to determine values of m and l_0 (Table III).

Fig 12 shows the distribution of glass fibre debond lengths as a function of the microstructure of a glass fibre/carbon/polyester hybrid. As we observed and reported earlier, the position of the extreme value distribution depends upon the ratio of carbon fibres to glass fibres. Closer examination of the two diagrams (fig 9 and 12) indicates that the relationship between the extreme value distribution and composition is not clear; the movement of cumulative probability curves as the ratio changes is not consistent from one hybrid to the other. In the case of glass fibres in epoxy, (without carbon fibres), the data are on the extreme right of the diagram, while for the polyester composite, the data are towards the extreme left. The pull-out lengths of glass fibres and carbon fibres remain essentially independent of microstructure (figs 13,14).

Values of m , l_0 and \bar{l} for the polyester hybrid composites are listed in Table IV. In the case of the debonding of glass fibres, m values are slightly higher for epoxy than polyester, while l_0 values are essentially independent of the choice of matrix.

For the extraction of broken glass fibres from their matrix sockets, values of m are similar for the two resins, while l_0 are less for the epoxy than polyester. The indication is that the interfacial bond strength between fibre and matrix is greater for the epoxy composite and, as we shall see later, the toughness is correspondingly lower.

3. MODELLING MICROMECHANISMS OF FRACTURE

Consider the propagation of a crack in a brittle matrix, around and beyond a long, strong fiber, glass fiber in polyester, for instance, (fig 15). Localised stresses at the tip of the crack are likely to cause a breakdown of the fibre-matrix bond. Under conditions of increasing load, the crack faces of the matrix separate and the

TABLE III

Values of m , l_0 , and \bar{l} for glass fibres and carbon fibres in epoxy resin

Ratio of C/G	Glass fibres debonding (mm)			Glass fibres pulling out (mm)			Carbon fibres pulling out (mm)		
	m	l_0	\bar{l}	m	l_0	\bar{l}	m	l_0	\bar{l}
0:100	6.9	5.6	5.3	2.4	0.26	0.23	-	-	-
13:87	4.5	4.9	4.4	2.0	0.36	0.25	1.3	0.35	0.32
23:77	4.2	4.9	4.4	2.1	0.24	0.22	2.0	0.31	0.28
37:63	5.3	5.1	4.7	1.6	0.24	0.23	2.0	0.37	0.32
44:56	5.8	6.7	5.9	1.8	0.32	0.27	2.4	0.30	0.33
54:46	9.1	5.6	5.3	1.7	0.30	0.26	2.6	0.39	0.34
64:36	4.8	4.7	4.3	1.9	0.31	0.27	2.2	0.34	0.31
70:30	5.0	4.1	3.8	2.2	0.31	0.28	2.2	0.32	0.28
83:17			2.3	3.4	0.21	0.19	2.2	0.25	0.22
100:0	-	-	-	-	-	-	2.4	0.31	0.28

TABLE IV

Values of m , l_0 , and \bar{l} carbon fibres and glass fibres in polyester

Ratio of C/G	Glass fibres debonding (mm)			Glass fibres pulling out (mm)			Carbon fibres pulling out (mm)		
	m	l_0	\bar{l}	m	l_0	\bar{l}	m	l_0	\bar{l}
0:100	3.6	5.2	4.7	2.5	0.35	0.31	-	-	-
23.77	3.4	6.6	5.8	2.0	0.53	0.45	2.7	0.42	0.37
37.63	4.1	5.1	4.7	2.7	0.46	0.41	4.2	0.48	0.44
64.36	4.0	6.7	6.0	2.8	0.41	0.37	3.0	0.42	0.37
70:30	3.7	5.3	4.7	2.5	0.49	0.43	2.6	0.38	0.34
100:0	-	-	-	-	-	-	2.7	0.37	0.33

interfacial debonded region, on either side of the matrix crack, extends. Relative displacement between fibre and matrix can then occur over the entire length of debonded fibre. Provided the fibre still interacts in some way with the matrix, by mechanical keying at the interface, for instance, a frictional (sliding) shear force is established soon after the bond fails. The distance over which this shear force acts is approximately equal to the product of the debonded length of fibre, l_d , and the differential failure strain of fibre and matrix, $\Delta\epsilon$. Since the initial frictional shear force, $\pi d(l_d/2)$, acts in each direction from the fracture surface of the matrix over a distance, $\Delta\epsilon l_d/2$, the work done per fibre is (3,5)

$$W_{pdf} = \pi d \tau l_d^2 \Delta\epsilon \quad (6)$$

$$= \pi d \tau l_d^2 \epsilon_f / 2 \quad (7)$$

provided $\epsilon_f \gg \epsilon_m$. This is a reasonable assumption for a brittle matrix which cracks at low strains. (d is the diameter of fibre).

The load on a fibre is a maximum in the debonded region and as it increases the fibre is likely to break at a flaw somewhere along its debonded length (fig 16). The localised elastic work of tensile deformation, W_d , in the fibre over a length, l_d , (sometimes referred to as fibre debonding energy (7)), can be expressed as

$$W_d = \pi d^2 \sigma_f^2 l_d / 8E_f \quad (8)$$

This equation does not account for the recoverable energy as the load builds up in the fibre over a distance $l_c/2$ from the point of fibre fracture* (8,9). σ_f and E_f are the tensile strength and Young's modulus of the fibre, respectively.

Provided there is some kind of interaction between the debonded fibre end and matrix, then a frictional (sliding) shear force opposes any applied force to extract the fibre (3,10), (fig 17). The total frictional work of the pull-out is

* A critical fibre length, l_c , is defined as the smallest length of fibre which, when embedded in a matrix, can be loaded to its breaking point.

$$W_p = \pi d \tau \ell_p^2 / 2 \quad (9)$$

The average work to extract a fibre whose embedded length lies between 0 and ℓ_p , is therefore

$$W_p = \pi d \tau \ell_p^2 / 6 \quad (\ell_p < \ell_c / 2) \quad (10)$$

assuming a constant frictional shear stress, τ .

The frictional shear stress can be estimated using the expression (6)

$$\tau = \sigma_f d / 2 \ell_c \quad (11)$$

In a fibre pull-out experiment, the maximum length of fibre that can be extracted from a block of matrix without first breaking is equal to $\ell_c / 2$. Equations 7 and 10 can be rewritten, therefore, in term of ℓ_d and ℓ_p ;

$$W_{pdf} = (\pi d^2 \sigma_f \epsilon_f / 8) \quad (\ell_d^2 / \ell_p) \quad (12)$$

$$W_p = \pi d^2 \sigma_f \ell_p / 24 \quad (13)$$

In each model, the work done is directly proportional to the number of fibres and each mechanism, in its own way, is sensitive to the interfacial shear stress. We have assumed that the interfacial shear stress is a constant. This may not be true; the frictional shear stress depends upon the radial force exerted by the matrix onto the fibre which is likely to be sensitive to the spacing between fibres and fibre bundles.

From the above relationships, we can identify three contributions to the total work to fracture the composite. The work to fracture the composite can be written in terms of ℓ_d and ℓ_p .

$$W_T = (\pi d^2 / 4) [(3 \sigma_f \epsilon_f) (\ell_d^2 / \ell_p) + (\sigma_f^2 \ell_d / E_f) + (\sigma_f \ell_p)] \quad (14)$$

where ℓ_d is the distance over which the fibre has debonded and ℓ_p is the maximum fibre pull-out length.

4. FRACTURE MECHANISM DIAGRAMS

In view of the agreement between the two methods of determining $\bar{\ell}$, the arithmetic means of fibre debond length and fibre pull-out lengths, together with the expressions of fracture energy, are used to estimate the energy of each mechanism of failure and total theoretical fracture energy of the composite. A diagram of fracture energy versus number

of glass fibres (fig 18) shows the estimated energy dissipated during the post-debond fibre sliding mechanism (equation 12). The relationship is not a simple linear one as one would expect from the form of the equation; the cumulative probability data showed fibre debond length to be sensitive to the number of fibres in the composite. We recall that it is the square of the fibre debond length and number of fibres which appears in the post-debond fibre sliding equation. The plateau to the curve reflects the reversal in the trend in shift of cumulative probability data for $N = 6400$ fibres to which reference was made earlier.

An estimation of the fibre debond energy (equation 8) is shown in the next diagram (fig 19). At first sight, the shape is linear but closer examination shows a smooth curve with a gradually increasing slope. It reflects the dependence of fibre debond length on the number of glass fibre strands. The plateau shown in the previous figure is less obvious since fibre debond energy is directly proportional to the length of debonded fibre. The energy dissipated in this way is significantly less than the work done in the post-debond fibre sliding mechanism.

The work to pull broken glass fibres out of a cracked matrix (equation 13) is of a similar order of magnitude as the fibre debond energy (fig 20). Both figures have a similar shape; the increase in gradient of the curve at the high numbers of fibres originates from the high values of fibre pull-out length shown previously in the cumulative probability data for $N = 8000$ fibres.

The result of summing these 3 energy parameters (equation 14) is shown in figure 21. Apart from a small rise in the curve at $N = 5000$ fibres, approximately, it is a smooth curve with a gradually increasing slope as the number of fibres increases. Comparison of the empirical diagram with experimental work of fracture data shows remarkable likeness in shape and magnitude (fig 22). From observations of the fracture of glass fibres in epoxy we know that the composite exhibits all the common modes of failure; matrix cracking, fibres debonding, fibres snapping and fibres pulling out. The dominant toughening mechanism appears to be post-debond sliding between fibre and matrix; the breakage of fibres and the pulling out of the broken fibre ends dissipates similar amounts of energy and together contribute little more than one-quarter of the total fracture energy of the composite.

The measured work of fracture of glass fibres in epoxy is 280 kJ/m^2 ,

approximately, and 200 kJ/m^2 after storing for 6 months.

Table V shows the predicted energy terms calculated using the models of fracture, together with average values of debond length and pull-out length of the glass fibres used in the calculation. In the mechanism involving debonding and slippage, aging has approximately halved the value of the post-debond fibre sliding parameter. The agreement between theoretical energy and experimental work of fracture is a good one.

Average values of fibre debond length and fibre pull-out length for the glass fibres and carbon fibres, combined with the equations of fracture energy, can be used to estimate the energy dissipated during fracture and pull-out of both kinds of fibre. In this case, fracture energy is plotted against percentage of carbon fibres in the hybrid composite (figs 23-28).

Figure 23 shows an estimation of the energy dissipated during glass fibre-matrix sliding soon after the bond has failed. While there is an overall decrease in energy as the carbon fibre content increases, as one would expect, it by no means forms a linear relationship. Certain features are worth pointing out. The first is that after a sharp drop in energy as glass fibre is replaced with carbon fibre, a plateau is observed up to 40% (by vol.) of carbon fibre. At that point, the fracture energy actually increases slightly before falling to zero as the remaining glass fibres are replaced with carbon fibres.

Recalling the cumulative probability data, we realize that it is the effects of composition on glass fibre debond length and the subtle balance between debond length and number of fibres which is the origin of the unexpected shape of the post-debond sliding energy diagram. The small peak in the diagram at 44% (by vol.) of carbon fibre coincides with the large displacement of the cumulative probability data to higher values of glass fibre debond length.

At first sight, glass fibre debond energy decreases linearly with an increase in volume fraction of carbon fibre (fig 24). Closer inspection shows a shallow curve with a very small peak at 44% (by vol.) of carbon fibre. Minor differences in shape and position of the cumulative probability curves are responsible for the non-linear behaviour.

Slight undulations in the pull-out curve for the glass fibres can also be indentified with minor changes in shape and position of the cumulative probability curves (fig 25). As a first approximation, the glass fibre debond energy and glass fibre pull-out energy are directly

TABLE V Effect of aging for 6 months upon the fracture energy
of a glass fibre-epoxy composite

	W_{pdf}	W_d (kJ/m ²)	W_p	W_T	W_{EXPT}
Before aging	226	46	56	328	280
After aging	117	34	58	209	202

These predictions are based on the following measurements:

$$\bar{l}_d \text{ (unaged) } = 5.3\text{mm}$$

$$\bar{l}_d \text{ (aged) } = 3.9\text{mm}$$

$$\bar{l}_p = 0.24\text{mm approximately, before and after aging}$$

It is the post-debond fibre sliding mechanism and the decrease in \bar{l}_d which appears to be primarily responsible for the decrease in work of fracture.

proportional to the amount of glass fibre in the composite, as one would expect from the form of the equations.

Similar undulations in the carbon fibre pull-out energy diagram originate in the small differences to be found in the cumulative probability data (fig 26). Ignoring these minor effects, the pull-out energy follows a linear relationship with carbon fibre content, as one would expect. Figs 27 and 28 show good agreement between theory and experiment.

GLASS FIBRES AND CARBON FIBRES IN POLYESTER

In this section, we present work of fracture data of a hybrid system with a polyester matrix. Data of mean fibre debond length and mean fibre pull-out length, together with the models of micro-mechanisms of fracture are used to estimate the energies dissipated during crack propagation (figs 29-33). Where possible, comparisons are made between the fracture behaviour of the two hybrid systems investigated and the effect of matrix becomes apparent.

Figure 34 shows the experimental work of fracture data for the two hybrid systems. Certain features of the curves are apparent. First, the general shape of the curves are similar and second, the polyester hybrid composites have work of fracture values which are about 50% higher than values obtained for the epoxy composites. One noticeable exception is the datum point for the glass fibre-polyester; in this case, the work of fracture is less than the value obtained for the epoxy composite. Certain comments can be made and generalisations drawn from comparison of the fracture energy diagrams for epoxy and polyester based composites. The overall shapes of the theoretical and experimental fracture energy curves are similar; and the relative order of magnitudes of the four energy parameters and the contribution each one makes to the total fracture energy or toughness of the composite are also alike. The shape of both total theoretical fracture energy curves is dominated by the post-debond fibre sliding term for glass fibres; and at the carbon fibre-rich end of the diagram, the pull-out term for carbon fibres is important. Comparison between the theoretical fracture energy and experimental work of fracture data show remarkable similarities in shape and magnitude. For glass fibre, the post-debond sliding energy term is a major component of the total fracture energy, while the debonding energy and pull-out energy terms are comparable in magnitude. Together, debonding and pull-out of glass fibre contribute no more than one-quarter of the total fracture energy of the hybrid composite.

On the other hand, carbon fibres were not observed to debond, and the work done in extracting them from a cracked matrix can be successfully equated to the fracture energy of a carbon fibre composite.

5. WORK OF FRACTURE OF STRUCTURAL FIBROUS COMPOSITES

Model specimens of the kind used in this study can be used to estimate the work of fracture of structural fibrous composites. Consider, for example, a structural unidirectional glass fibre or carbon fibre composite, fabricated to the dimensions of the model composite, 20 mm x 10 mm x 2 mm. If the fibre volume fraction is 0.5, then the total cross-sectional area of the fibres is $10 \times 10^{-6} \text{ m}^2$. In a model composite containing 5 tows of carbon fibres, for instance, the total cross-sectional area of the fibres is $1.4 \times 10^{-6} \text{ m}^2$, approximately. There are about 7 times as many fibres in the structural composite compared to the model composite. If we multiply the measured fracture energy of the model carbon fibre composite by 7 times, and in the case of the model glass fibre composite containing 5 strands by 8.5 times, we can estimate the work done in breaking the structural composite. The work of fracture of the structural composite is calculated by simply dividing the estimated work to break the specimen by twice its cross-sectional area. Table VI lists the work of fracture of several carbon fibres and glass fibre structural composites estimated in this way. They are based on measurements of work of fracture obtained using the model composite specimens. These values are very close to measurements made by others using fracture mechanics specimens, (see, for example, Harris and Bunsell (11) and Beaumont and Phillips (12)), but in those cases a detailed failure analysis was not carried out and would have been extremely difficult to have done so.

6. HYGROTHERMAL AGING EFFECTS

Weight Changes

Exposure to extremes of humidity at 100°C results in a change of weight (ΔW) with time (t), of epoxy, glass fibre-epoxy and carbon fibre-epoxy (Fig 35). The initial slope of a weight versus (time)^{1/2} curve for matrix and composite aged at 95% RH is linear. It suggests that the diffusion of water is Fickian controlled, i.e., $\Delta W \propto t^{1/2}$. Complete saturation is achieved after 5 days, approximately, corresponding to a water content of about 3 %/0. In fig 35, data are normalised to the

TABLE VI

	<u>Work of fracture (kJ/m²)</u>
Carbon fibre/epoxy	48
64% Carbon fibre/36% glass fibre/epoxy	75
Glass fibre/epoxy	148
Carbon fibre/polyester	70
64% Carbon fibre/36% glass fibre/polyester	118
Glass fibre/polyester	132

(The nominal fibre volume fraction is 0.5)

volume fraction of epoxy. The superposition of data indicates that the diffusion mechanism is in some way determined by the matrix. In contrast, aging of epoxy and composite at 100°C, 0% RH results in a decrease in weight. We believe a loss of volatiles from the epoxy takes place. An additional weight loss of the composite may be due to drying out of the glass fibres and carbon fibre originating as moisture absorbed onto the surface of the fibre before impregnation with resin.

Cumulative Probability Diagrams of Failure Data

Failure data of fibre debond length and fibre pull-out length collected in the fractographic analysis are presented in the following cumulative probability diagrams (fig 36-41). In Fig 36 are shown data of debond length of glass fibres in epoxy after aging at 100°C, 0% RH. Each distribution of data do not superimpose but are displaced relative to one another. Inspection of positions of sets of failure data reflect the observed variations in shape of the experimental work of fracture curve. For example, specimens tested after manufacture ($t = 0$) produce failure data which fall towards the right of the probability diagram, or have high values of fibre debond length. Failure data collected after 1 h are on the left of the diagram and correspond to low values of debond length. Each subtle movement of a set of data to higher and lower values of debond length for aging times between 1 h and 28 days correlate with a rise and fall of the curve drawn through the measurements of work of fracture. The Weibull constant m describes the spread of failure data for each aging cycle (Table VIII). For an aging time of 10 days $m = 3$. and between 2 and 4 weeks $m = 2$, approximately. The difference may not be significant, but when considered together with the shift of failure data with time, a change in m may suggest a variation in mechanism of failure.

The distribution of failure data to describe the extraction of broken glass fibre ends is shown in fig 37. The data fall in a narrow band with superposition at low probabilities and low values of fibre pull-out length, with slightly displaced data at $P = 1$. In general, a slight variation in shape and position of a probability curve reflects the observed changes in work of fracture with time. For $t = 1$ h, failure data lie close to the left of the band. After 1 day, the distribution has moved to the right side of the band which is later displaced to lower values of pull-out length as t approaches 10 days. For aging between

2 and 4 weeks, the probability curve moves again to higher values of pull-out lengths of fibres. An anomaly may exist for data corresponding to $t = 0$ which lie in the centre of the band instead of to the right as we observe for the distribution of measurements of fibre debond length. The Weibull constant m ranges between 1.8 and 2.5 (Table VII).

We do not observe any debonding of carbon fibres although the fibres do pull-out after snapping at flaws. The distribution of pull-out lengths fall in a narrow band with the superposition of data at low probabilities and separation of data at $P = 1$ (fig 39). The shortest pull-out lengths are observed at $t = 0$ and $t = 7$ days; the longest fibres are found at times of 1 day, 10 days and 14 days. Each movement of the distribution of data is consistent with observed variations in work of fracture as a function of time. The Weibull constant m lies between 1.8 and 2.5, similar to values corresponding to the pulling out of glass fibres (Table VIII).

Cumulative probability diagrams displaying failure data of glass fibres and carbon fibres in epoxy at 100°C , 95% RH are shown in figs 39-41. Data essentially superimpose for exposure times up to 1 week and are located between distribution curves for $t = 0$ and $t = 2-3$ weeks. The data corresponding to $t = 1$ h and $t = 10$ days are between the distribution curves for 1 week and 2 weeks. The positions of the probability curves illustrate the time-dependence of the debonding process of glass fibres. At $t \leq 1$ h, the fibre debond length decreases; between 1 h and 3 days, the length increases; and between 3 days and 2 weeks, the length decreases once more. We see that m is between 2.0 and 2.4 and $m = 3.3$ for data collected in the first 10 days and following 2 weeks of aging, respectively (Table VII). The distribution of fibre pull-out data fall in narrow bands (figs 40,41). Close inspection shows slight displacements of the probability curves to lower values of pull-out length with time to a similar extent that we observed data collected in a dry environment. The Weibull constant m is between 2.0 and 2.6 for both composite systems (Table VII).

Work of Fracture

The work of fracture data for composites aged at 100°C , 0% RH are shown in Fig 42. For glass fibres in epoxy, a precipitous fall in toughness by nearly one-half occurs after 1 h. This drop in toughness is almost recovered after 1 day but the toughness falls during again during the next 150 h or so. Aging for 1 week produces a minimum in the work of fracture curve of ca. 80 kJ/m^2 . Over the next 3 weeks or so, we see

TABLE VIII Values of the Weibull constant m for the debonding and pulling out of glass fibres and the pulling out of carbon fibres in epoxy

Time (h)	Debonding glass (100°C, 0% RH)			Debonding glass (100°C, 95% RH)		
	glass	Pull-out glass	carbon	glass	Pull-out glass	carbon
0	2.9	2.4	2.3	2.9	2.4	2.3
1	3.5	2.5	2.0	2.2	2.2	2.2
24	2.9	2.0	2.0	2.2	2.2	2.6
72	3.1	2.1	2.3	2.4	2.4	2.0
168	3.0	2.5	2.0	2.4	2.3	2.4
240	3.0	1.9	1.8	2.0	2.5	2.6
336	2.1	1.8	2.5	3.3	2.4	2.5
672	2.4	1.8	2.5	3.2	2.5	2.6

a steady rise in toughness towards the original value. For carbon fibres in epoxy, an initial increase in work of fracture after 1 h is followed by a gradual decrease to a constant value of ca. 40 kJ/m^2 after 100 h, approximately.

Exposure of glass fibre-epoxy to 100°C , 95% RH for 1 h causes the work of fracture to fall by nearly one-fifth to ca. 95 kJ/m^2 (fig 43). The initial work of fracture is recovered after 3 days before falling over the next 2 weeks to a value of ca. 65 kJ/m^2 . The data collected for carbon fibres in epoxy shows a trend similar to the one observed during aging at 100°C , 0% RH. The maxima and minima in the work of fracture can be identified with the subtle movement of the failure data.

The open symbols of figs 42, 43 are theoretical values of work of fracture based on the models and failure data. In all cases, there is excellent agreement between the experimental work of fracture and predicted fracture energy, although in general, theory overestimates the measurement of toughness.

Similarity between the work of fracture data and predicted values of fracture energy suggests that it is the energy dissipated during extraction of broken carbon fibres behind the tip of a crack that is the origin of toughness of carbon fibres in epoxy. The dissipation of energy during slippage of unbonded glass fibres close to a crack tip, and their subsequent extraction behind an advancing crack front can be equated to the work to fracture glass fibres in epoxy. In both systems, the fall in toughness with time at 100°C , 0% RH can be attributed to an improvement in bond strength. This can occur as a result of additional post-curing of the resin and contraction around the fibre. Such an "aging effect" manifests itself in a reduction in debond length of glass fibres, and a slight decrease in pull-out length of glass fibres and carbon fibres. These observations explain the larger reduction in toughness of the glass fibre composite.

The origin of the increase in toughness of glass fibres in epoxy after aging for 2 weeks at 100°C , 0% RH is unclear. We observe an increase in length over which the fibre debonds and a change in value of m , with little change in pull-out length. The inference is that the interfacial shear strength has decreased, perhaps due to degradation of the interface by some means. It may be that the chemical bond between glass fibre and matrix is weakened as a result of polymerisation of the silane coupling agent on the surface of the fibre (13).

A fall in work of fracture of both composite systems aged at 100°C , 95% RH for $t > 3$ days corresponds to a shift of fibre debond length and

and fibre pull-out length data to the left of the probability diagram, ie, to shorter lengths. This may be attributed to an enhancement of interfacial shear strength as a result of moisture absorption and matrix swelling and an increase in radial compressive force of the matrix onto the fibres. We see from the fibre pull-out models, that an increase in bond strength reduces the fibre pull-out length and pull-out energy as we observe. The collection of failure data and their relative positions to one another in the probability diagram support this hypothesis for $t > 3$ days.

The precipitous fall in work of fracture of the glass fibre composites at $t \leq 1$ h at 100°C , 0% RH corresponds to positional changes of the probability curves of failure data to lower values. The effect is also observed after annealing in the humid environment. Because of the short time involved, we believe that the effect is a thermal one. It may be that a moist surface of the fibres before impregnation with resin is drying out, an effect which is more pronounced in air at 0% RH. Alternatively, the short annealing treatment may cause relaxation of any residual stress in the matrix which affects the bond strength. Whatever the reason, the two composite systems behave differently at $t \leq 1$ h and the nature of the phenomenon is unknown to us at this time.

ACKNOWLEDGEMENTS

We wish to acknowledge the support of the Air Force Office of Scientific Research, Washington, D.C., under grant number AFOSR-78-3644.

REFERENCES

1. J.N. Kirk, M. Munro and P.W.R. Beaumont, *J. Mater. Sci.* 13 (1978) 2197.
2. M. Munro and P.W.R. Beaumont, *Third International Conference on Mechanical Behaviour of Materials*, 3 253, Cambridge, August 20-24, 1979, Editors - K.J. Miller and R.F. Smith, Published by Pergamon Press (U.K.).
3. A. Kelly, *Proc. Roy. Soc.* 319A (1970) 95.
4. P.W.R. Beaumont and B. Harris, *J. Mater. Sci* 7 (1972) 1265.
5. B. Harris, J. Morley and D.C. Phillips, *J. Mater. Sci* 10 (1975) 2050.
6. A.S. Argon and F.A. McClintock, *Mechanical Behaviour of Materials*, Published by Addison-Wesley, 1966, Massachusetts, U.S.A.
7. J.O. Outwater and M.C. Murphy, *Modern Plastics* 7, 160, (1970).
8. M.R. Piggott, *J. Mater. Sci.* 5, 669 (1970).
9. J. FitzRandolph, D.C. Phillips, P.W.R. Beaumont and A.S. Tetelman, *J. Mater. Sci.* 7, 289, (1972).
10. A.H. Cottrell, *Proc. Roy. Soc.* A282, 2, (1964).
11. B. Harris and A.R. Bunsell, *Composites*, 6, (1975), 197.
12. P.W.R. Beaumont and D.C. Phillips, *J. Composite Materials*, 6 (1972) January.
13. H. Ishida and J.L. Koeing, *J. Poly. Sci.*, 17 (1979) 615.

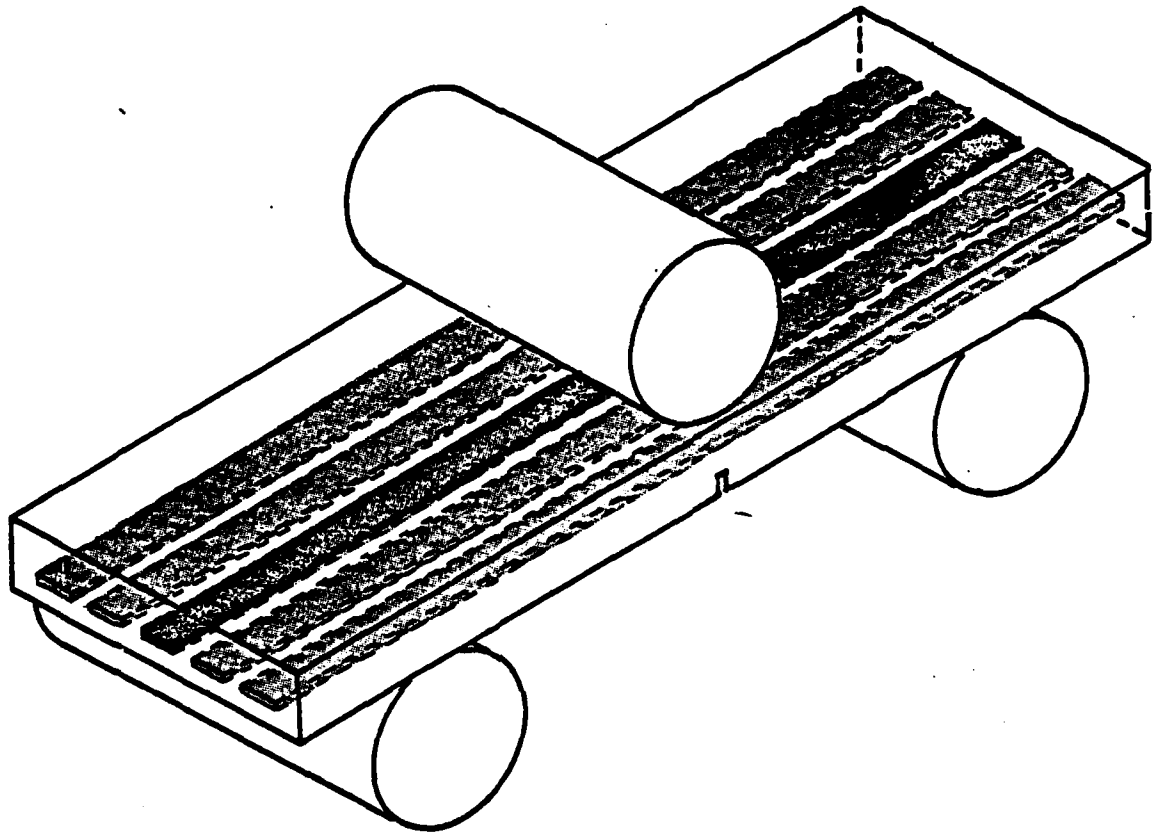
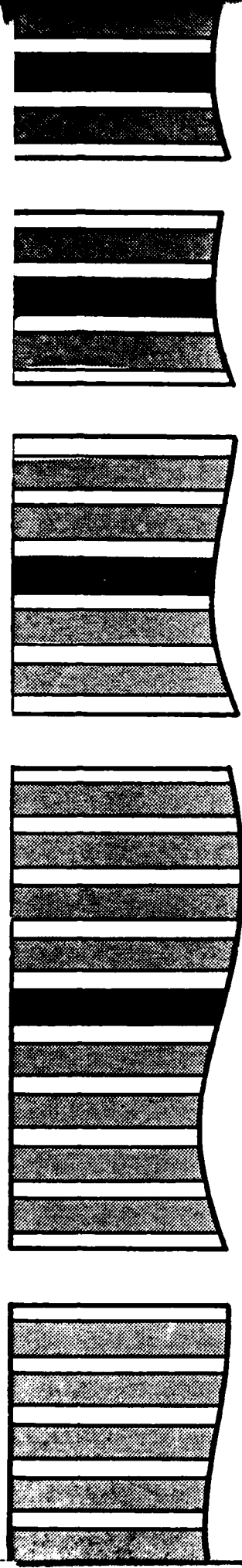


Fig. 1 A bar of transparent resin containing a single layer of unidirectional hybrid tape close to the tensile face in a 3-point bend test. (Dimensions of the specimen are 200 mm \times 10 mm \times 2 mm).



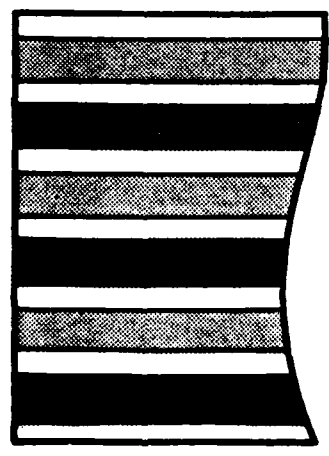
0

13

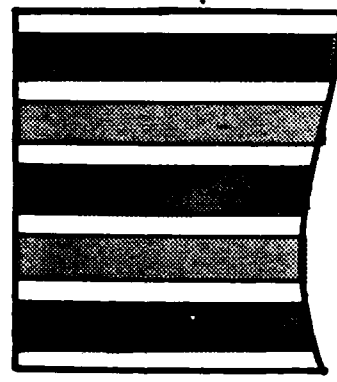
23

37

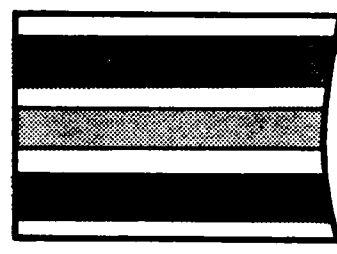
4



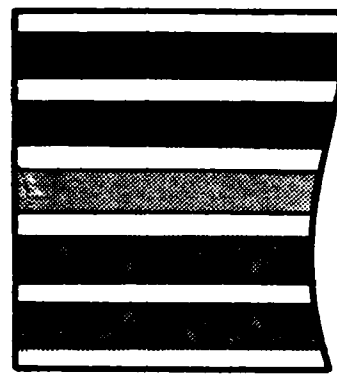
54



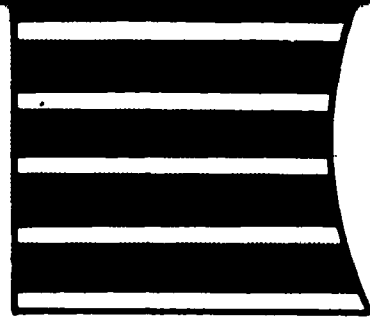
64



70



83



100

Fig. 2 Various combinations of carbon fibre and glass fibre bundles in unidirectional hybrid tapes used in the manufacture of model specimens.

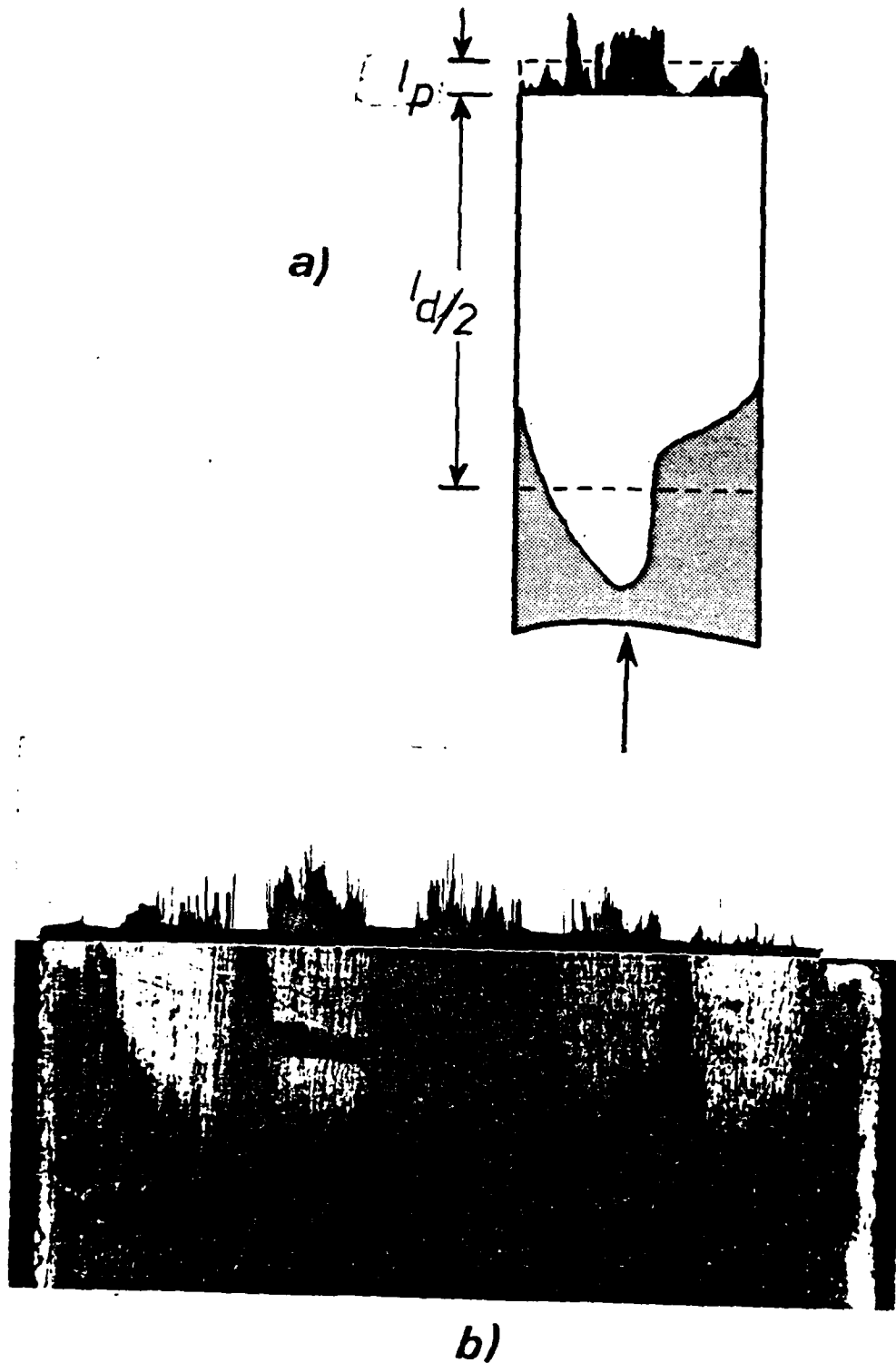


Fig. 3 A photomicrograph (b) of a central tow of carbon fibres with two strands of glass fibres on either side. The broken half of a specimen shows profiles of pulled-out fibres (dark regions) and debonded fibres (light regions). The sketch (a) represents the pulled-out and debonded fibre of one of the glass fibre strands, defining l_p and l_d .

CUMULATIVE PROBABILITY (P)

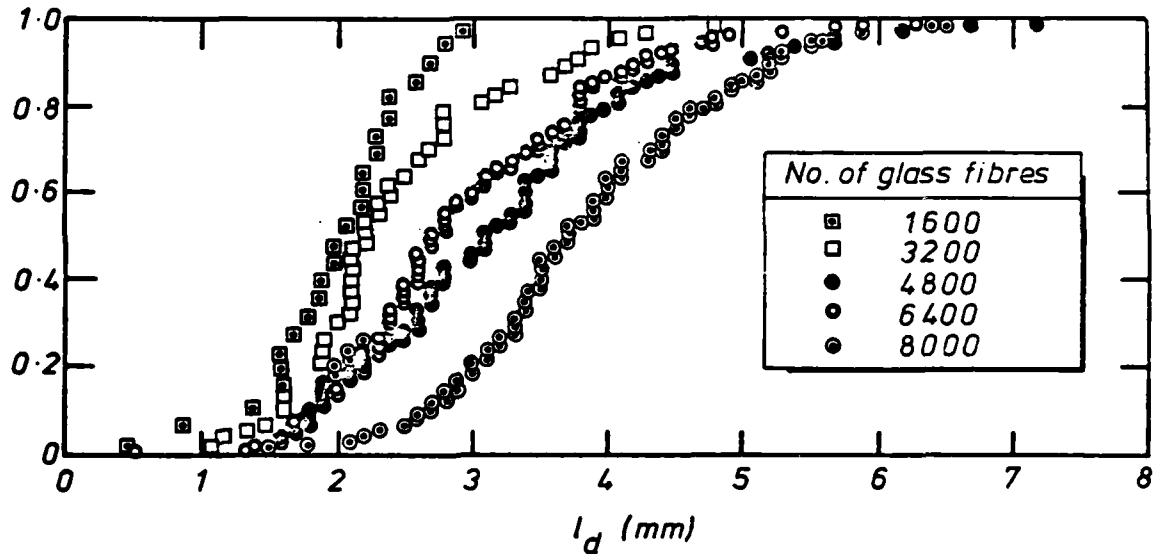


Fig. 4 Extreme value distributions of lengths of debonded glass fibres in epoxy for different numbers of strands in the model specimens. (1 strand contains 1600 filaments, 2 strands contains 3200 filaments, and so forth.)

In this diagram and other cumulative probability diagrams shown in this report, about 300 datum points collected from between 15 and 20 duplicate specimens and tests, constitute a single cumulative probability curve.

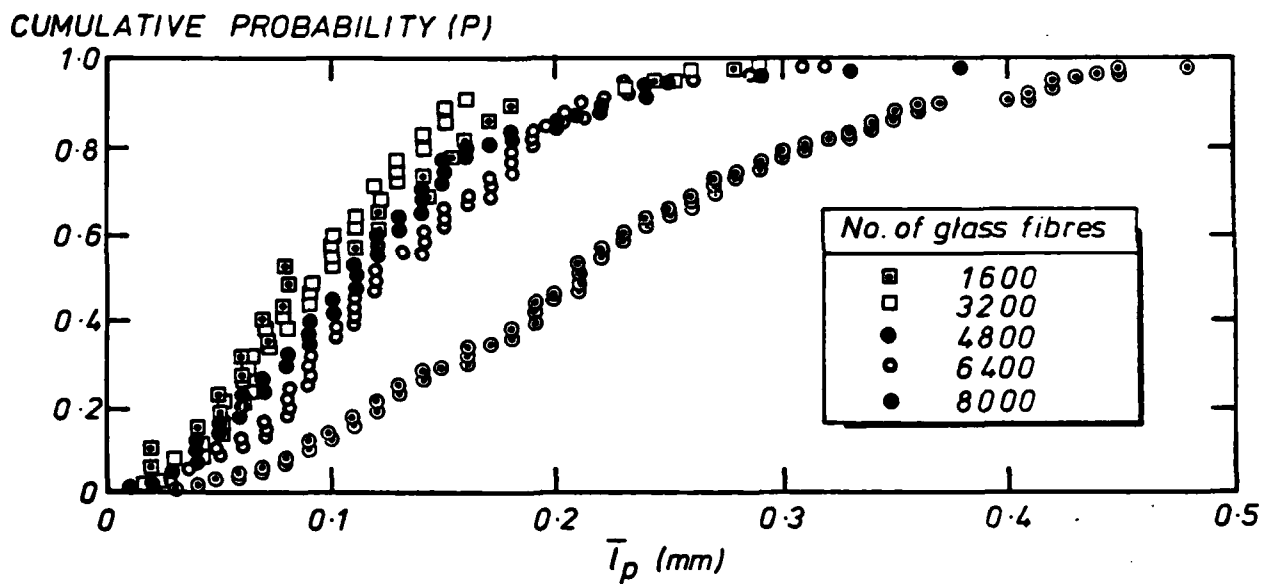


Fig. 5 Extreme value distributions of lengths of pulled-out glass fibres in epoxy.

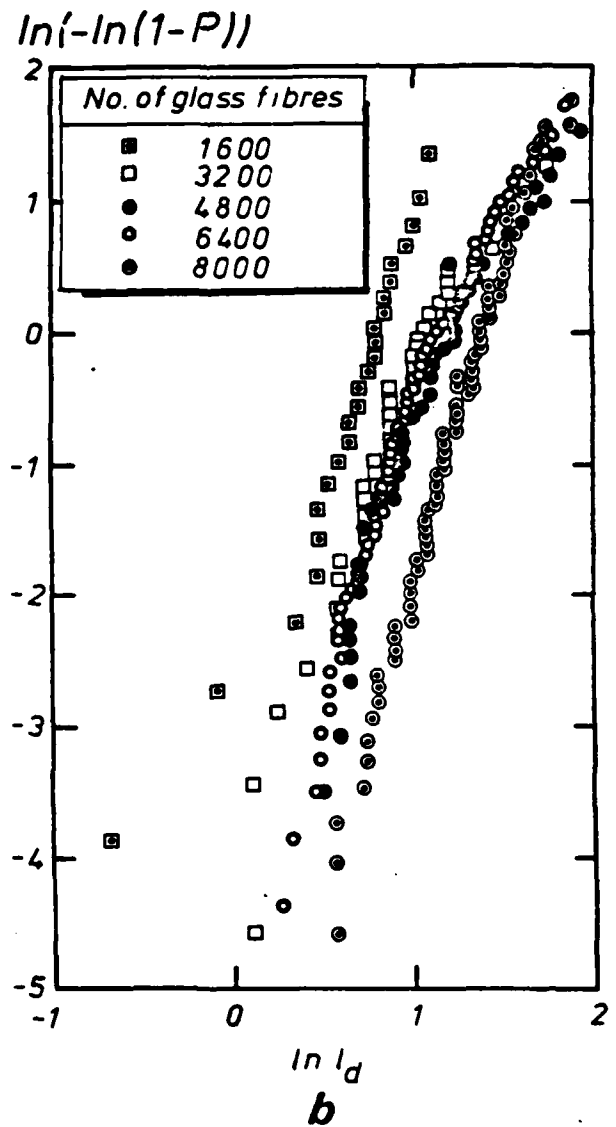
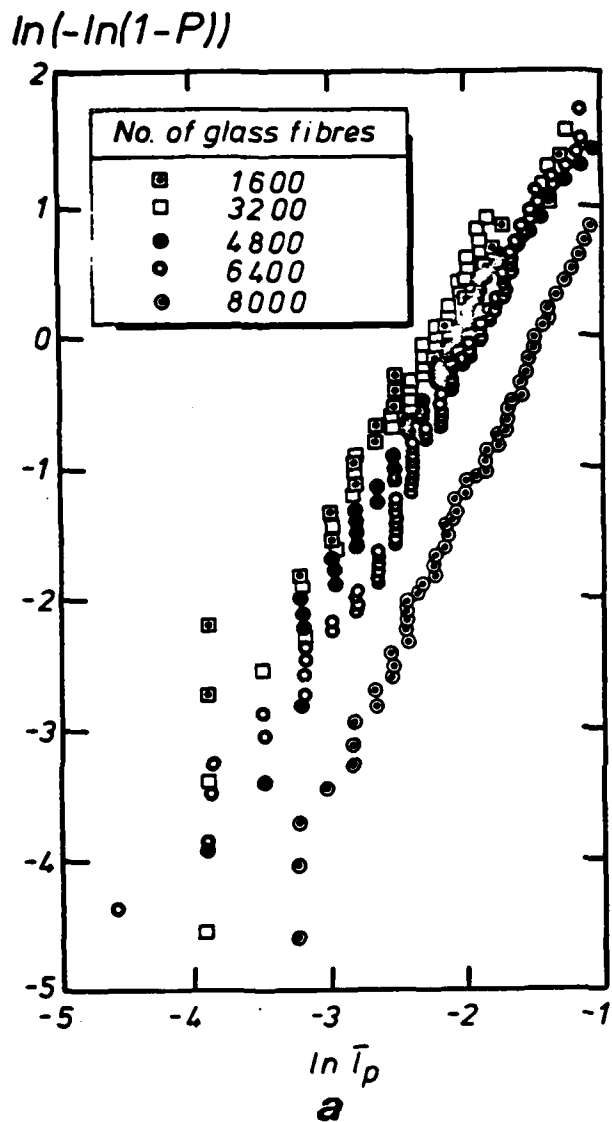


Fig. 6 Logarithmic plots of the data presented in Figs. 4 and 5.

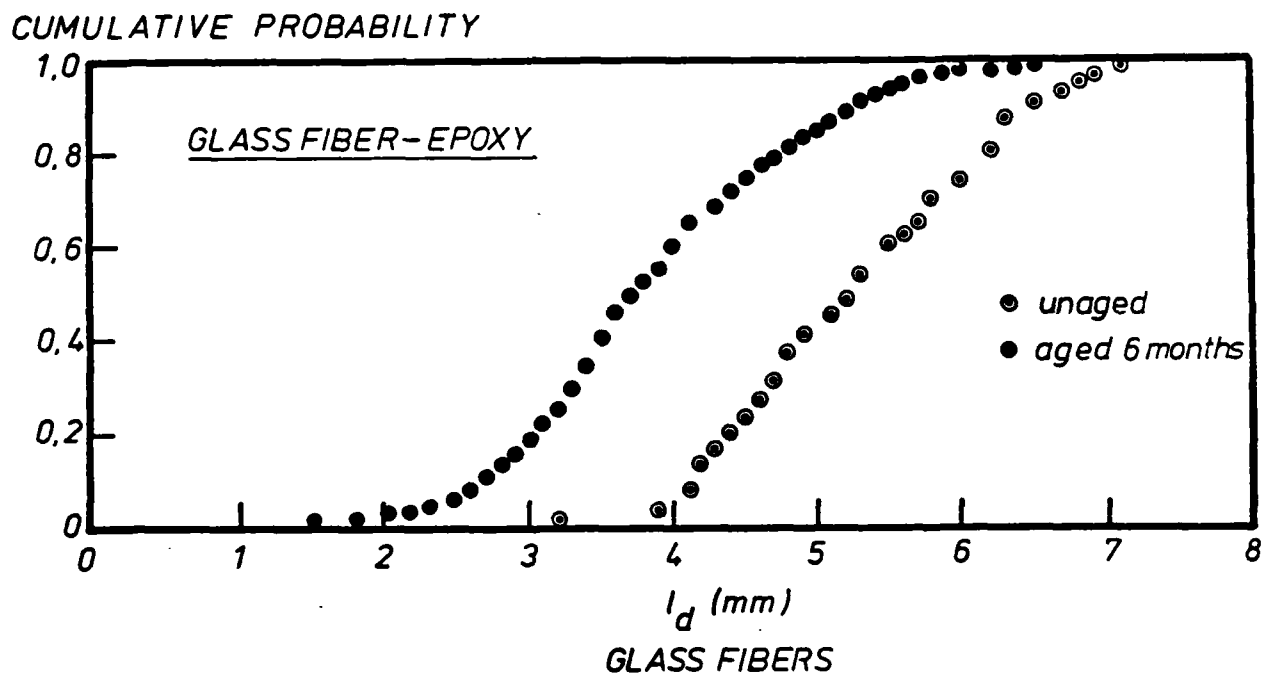


Fig. 7 Extreme value distribution of lengths of debonded glass fibres in epoxy before and after aging for 6 months at $18 (+2) ^\circ\text{C}$, $65 \pm \text{RH}$.

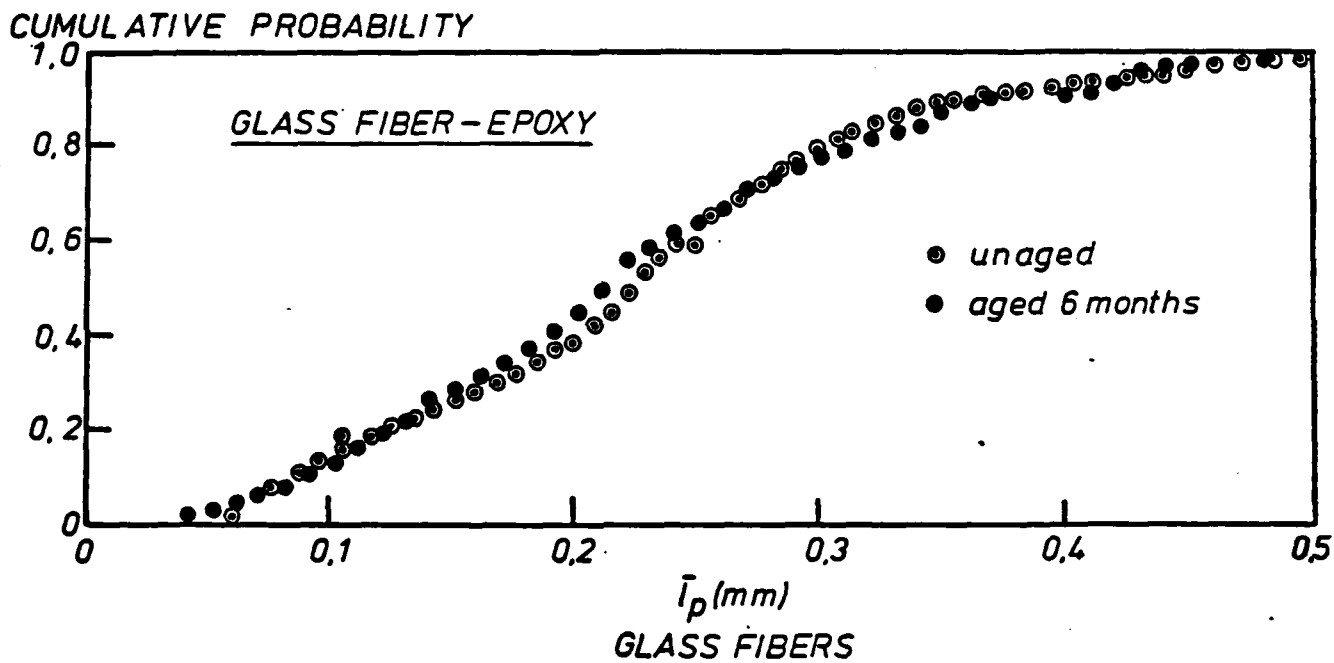


Fig. 8 Extreme value distributions of lengths of pulled-out glass fibres in epoxy before and after aging for 6 months at $18 (\pm 2) ^\circ\text{C}$, 65 % RH.

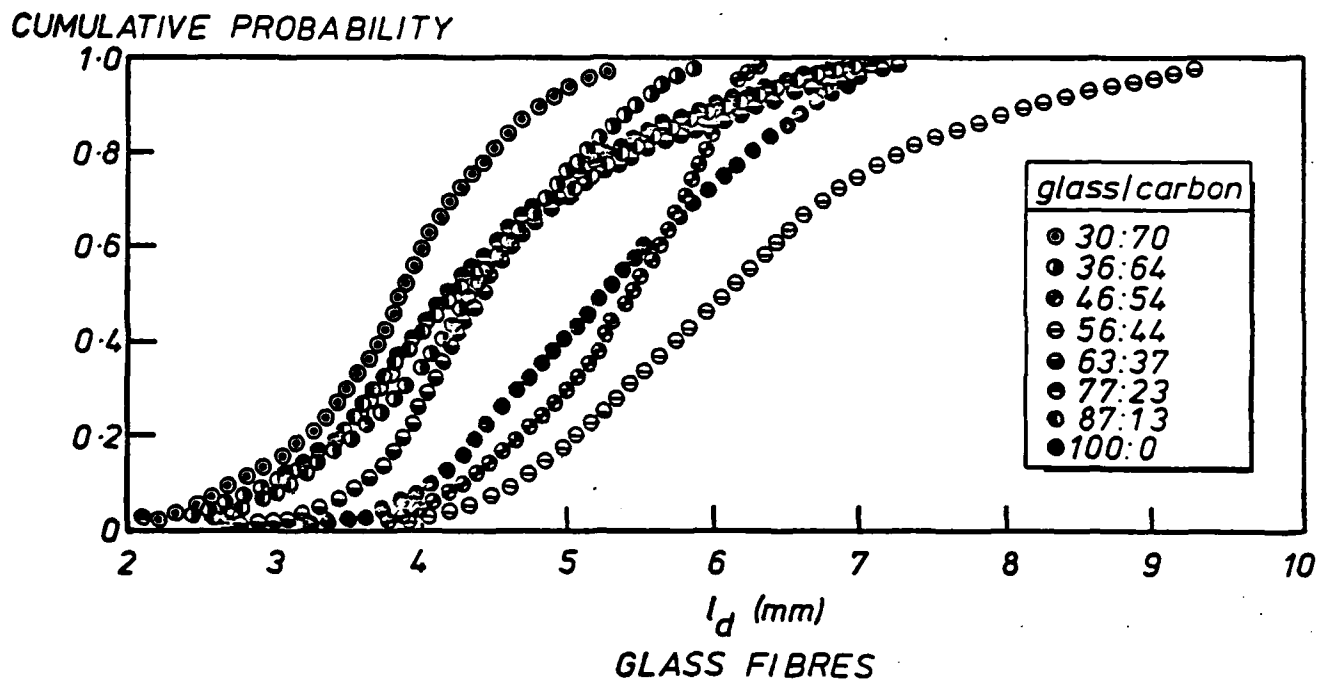
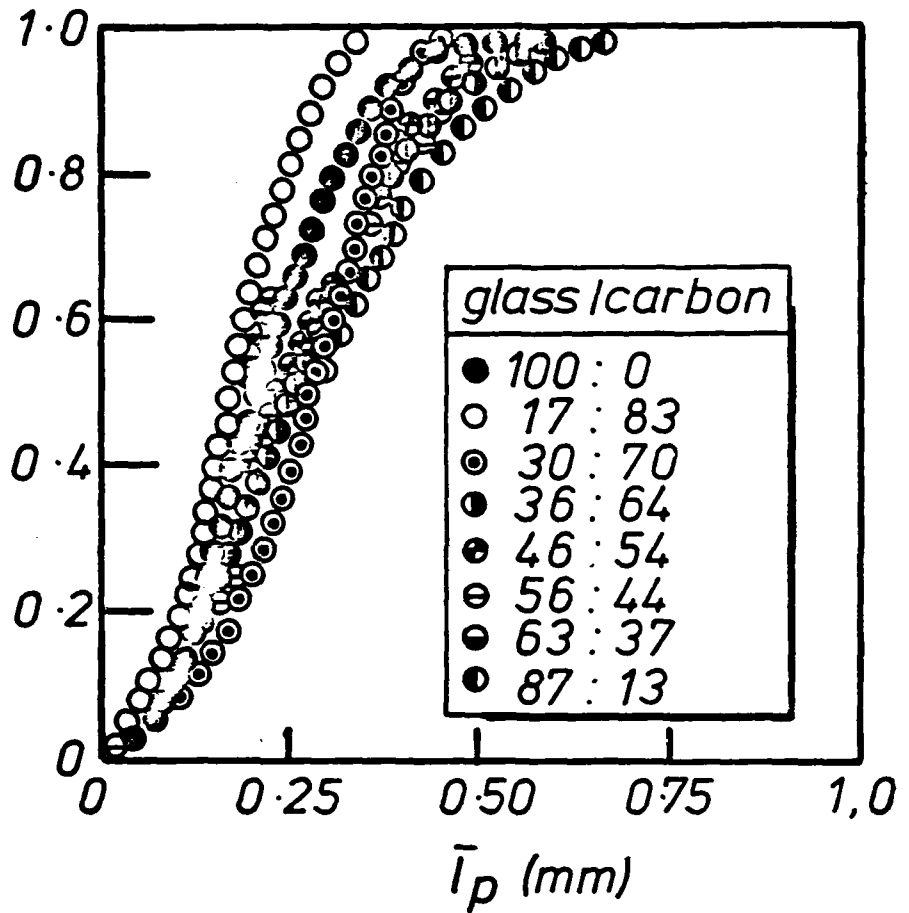


Fig. 9 Extreme value distributions of lengths of debonded glass fibres in hybrid composites (epoxy matrix).

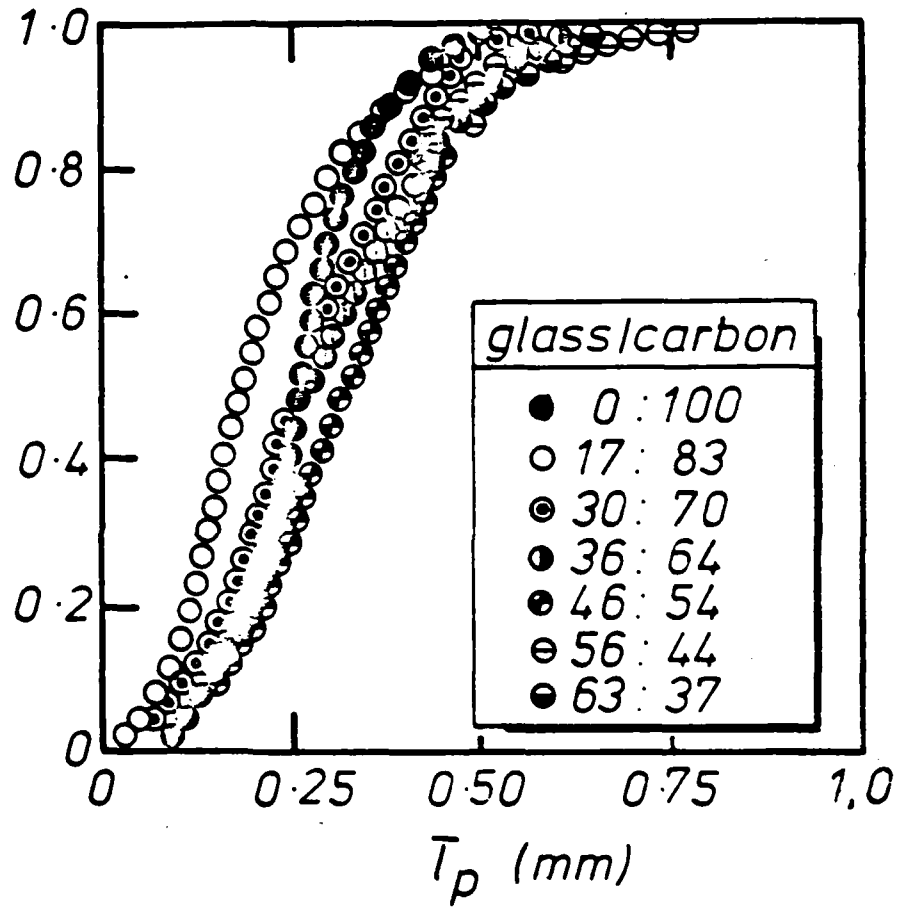
CUMULATIVE PROBABILITY



GLASS FIBRES

Fig. 10 Extreme value distributions of lengths of pulled-out glass fibres in hybrid composites (epoxy matrix).

CUMULATIVE PROBABILITY



CARBON FIBRES

Fig. 11 Extreme value distributions of lengths of pulled-out carbon fibres in hybrid composites (epoxy matrix).

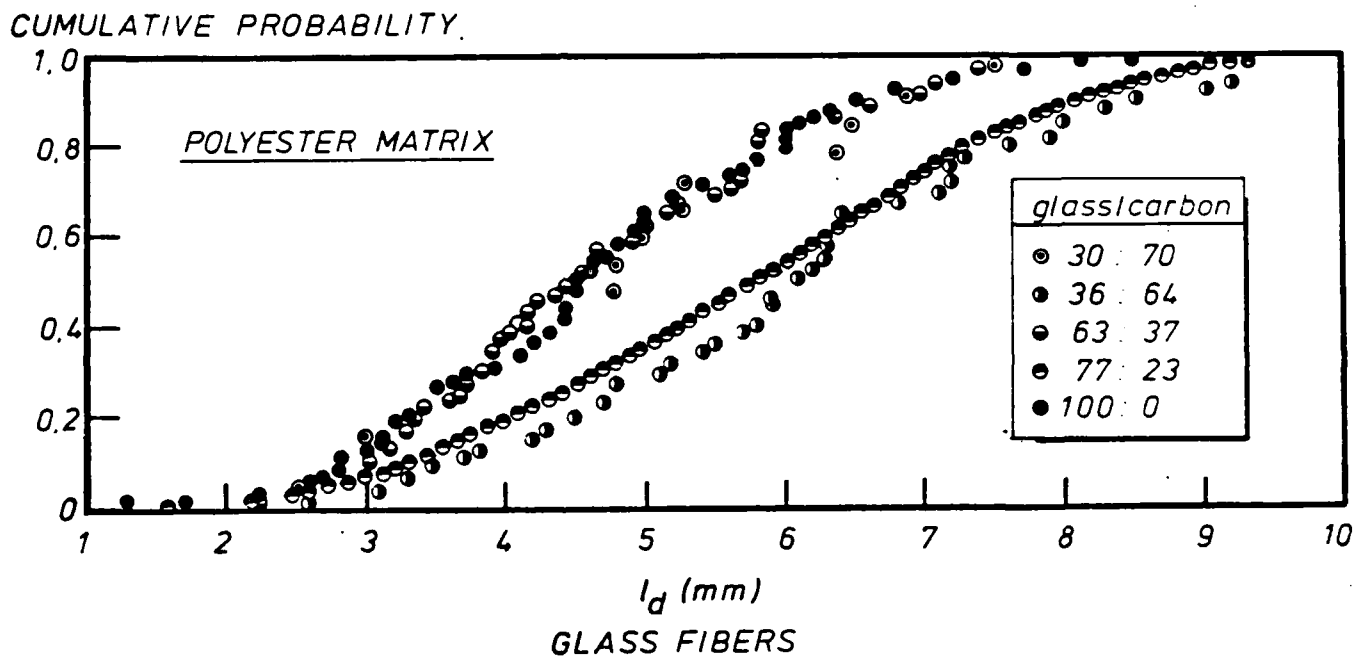


Fig. 12 Extreme value distributions of debonded lengths of glass fibres in hybrid composites (polyester matrix).

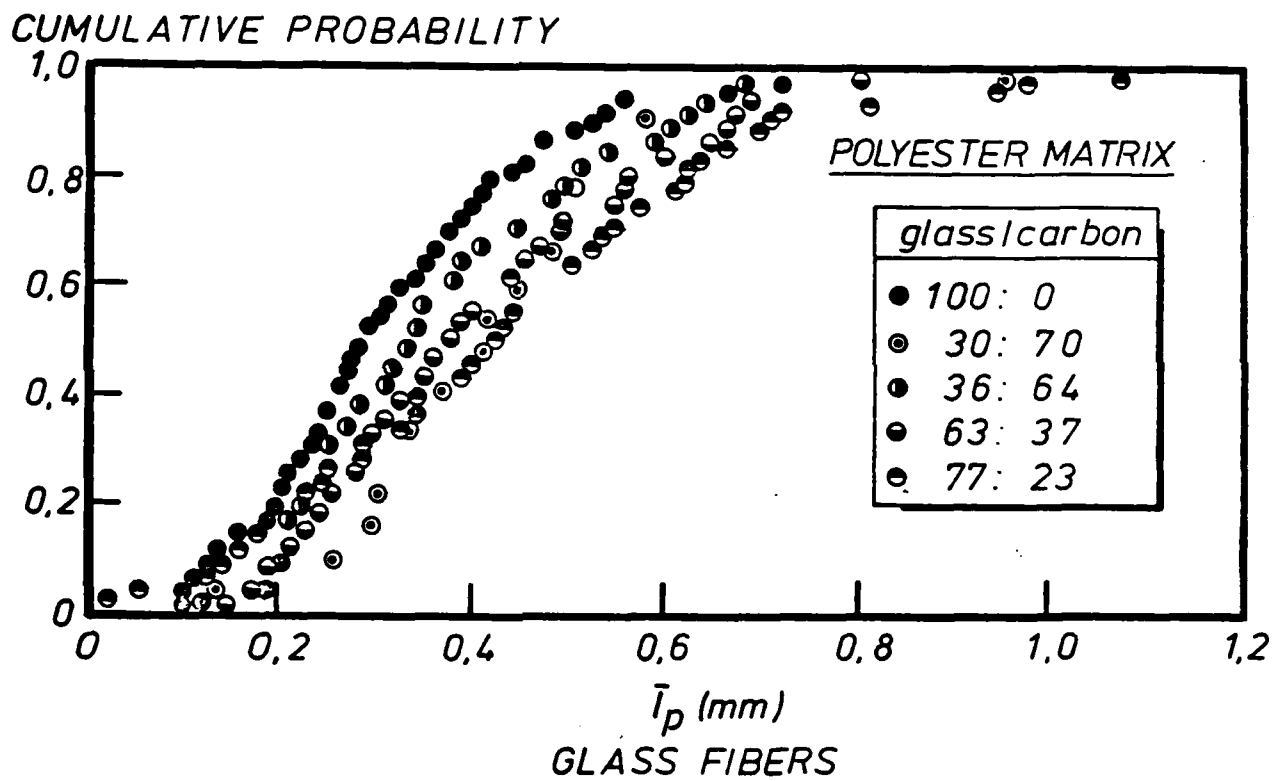


Fig. 13 Extreme value distributions of pulled-out lengths of glass fibres in hybrid composites (polyester matrix).

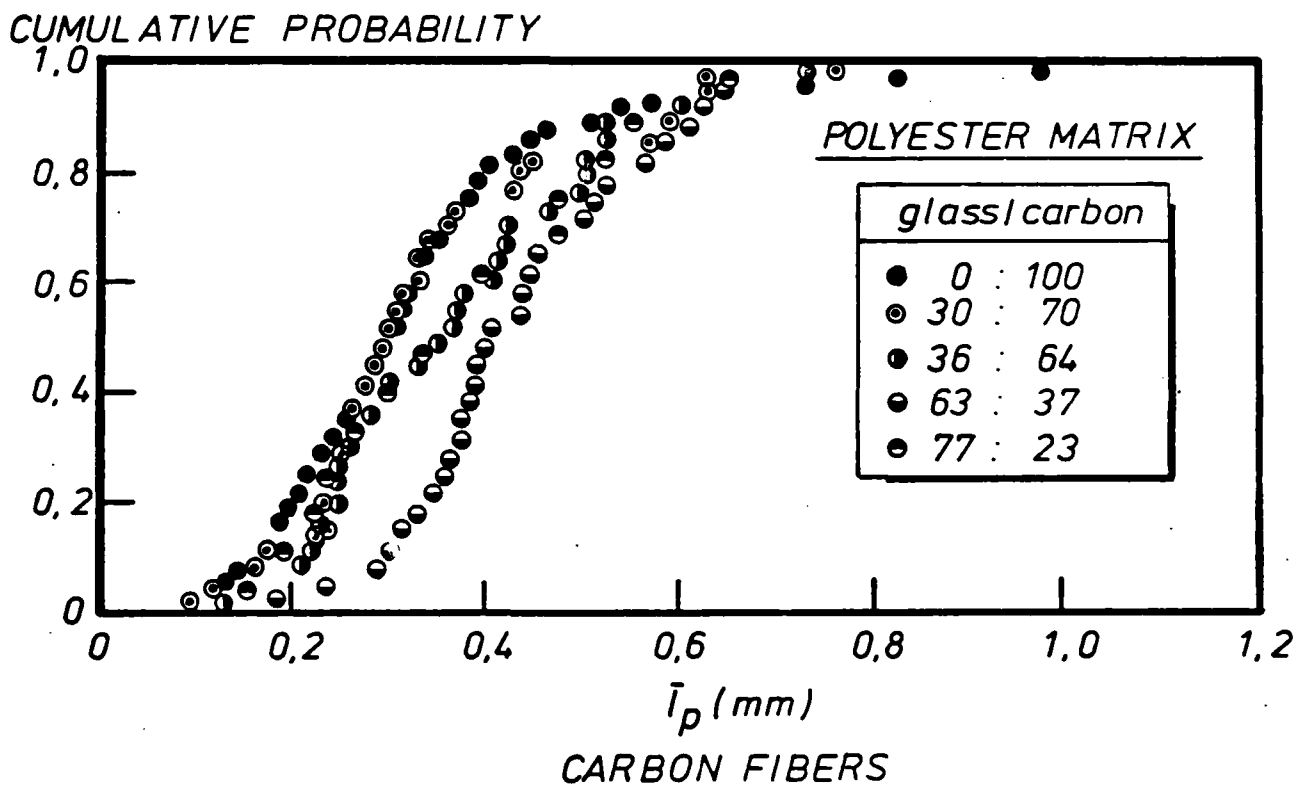
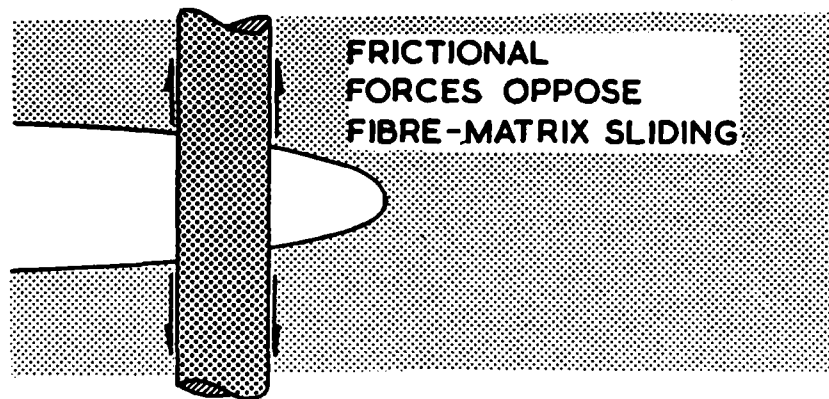


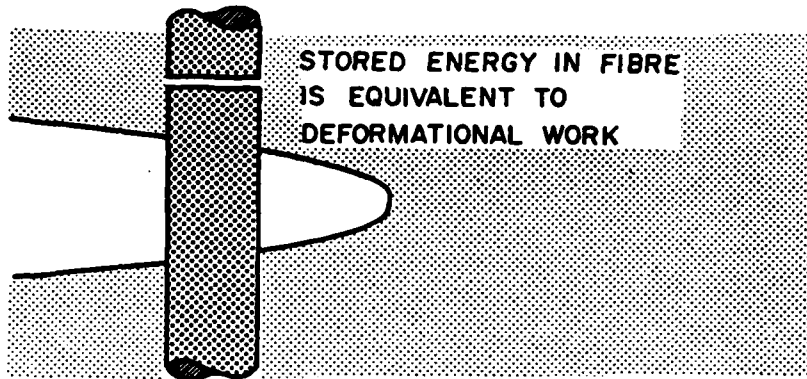
Fig. 14 Extreme value distribution of pulled out lengths of carbon fibres in hybrid composites (polyester matrix).



$$W_{pdf} = \frac{\pi d \tau l_d^2 \Delta \epsilon}{2}$$

a

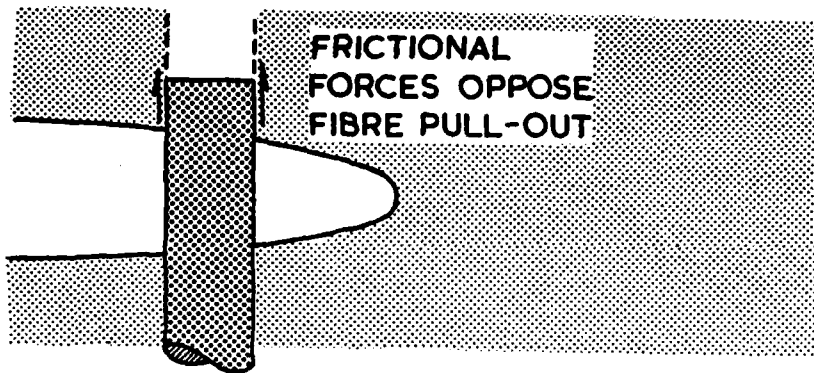
Fig. 15 A loaded fibre debonds and slips in the matrix socket behind an advancing crack front.



$$W_d = \pi d^2 \sigma_i^2 l_d / 8 E_i$$

b

Fig. 16 An overloaded fibre snaps at a weak point in the debonded region of the fibre as the crack front advances.



$$W_p = \pi d \tau l_p^2 / 6$$

C

Fig. 17 A broken fibre pulls-out of its matrix socket as the fracture surfaces of the cracked matrix separate.

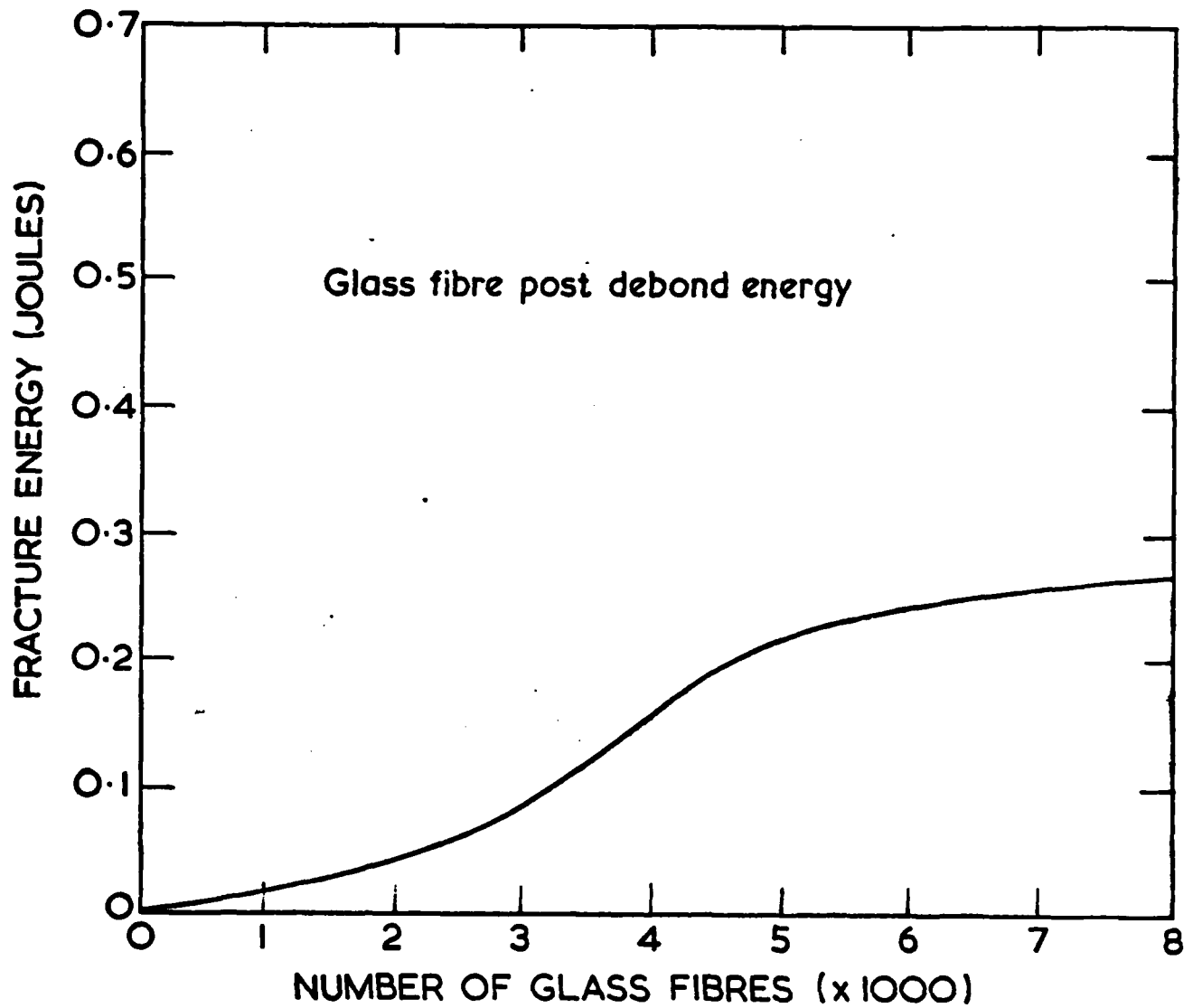


Fig. 18 An estimation of the energy dissipated during post-debond sliding of glass fibres in their epoxy matrix sockets, based on data of fibre debond length and fibre pull-out length, together with eq. (12).

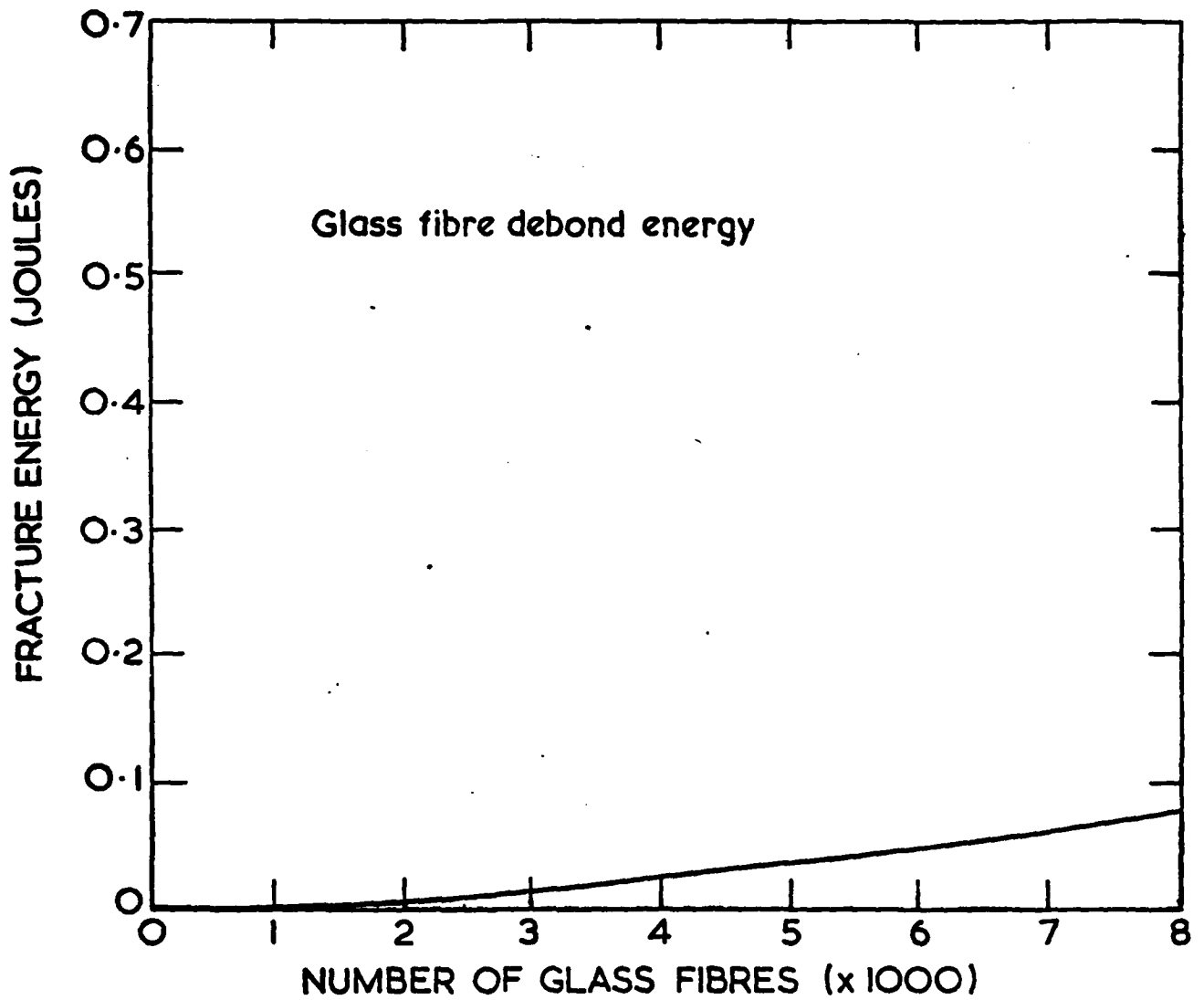


Fig. 19 An estimation of the release of stored elastic strain energy when a debonded glass fibre snaps, based on data of fibre debond length, together with eq. (8).

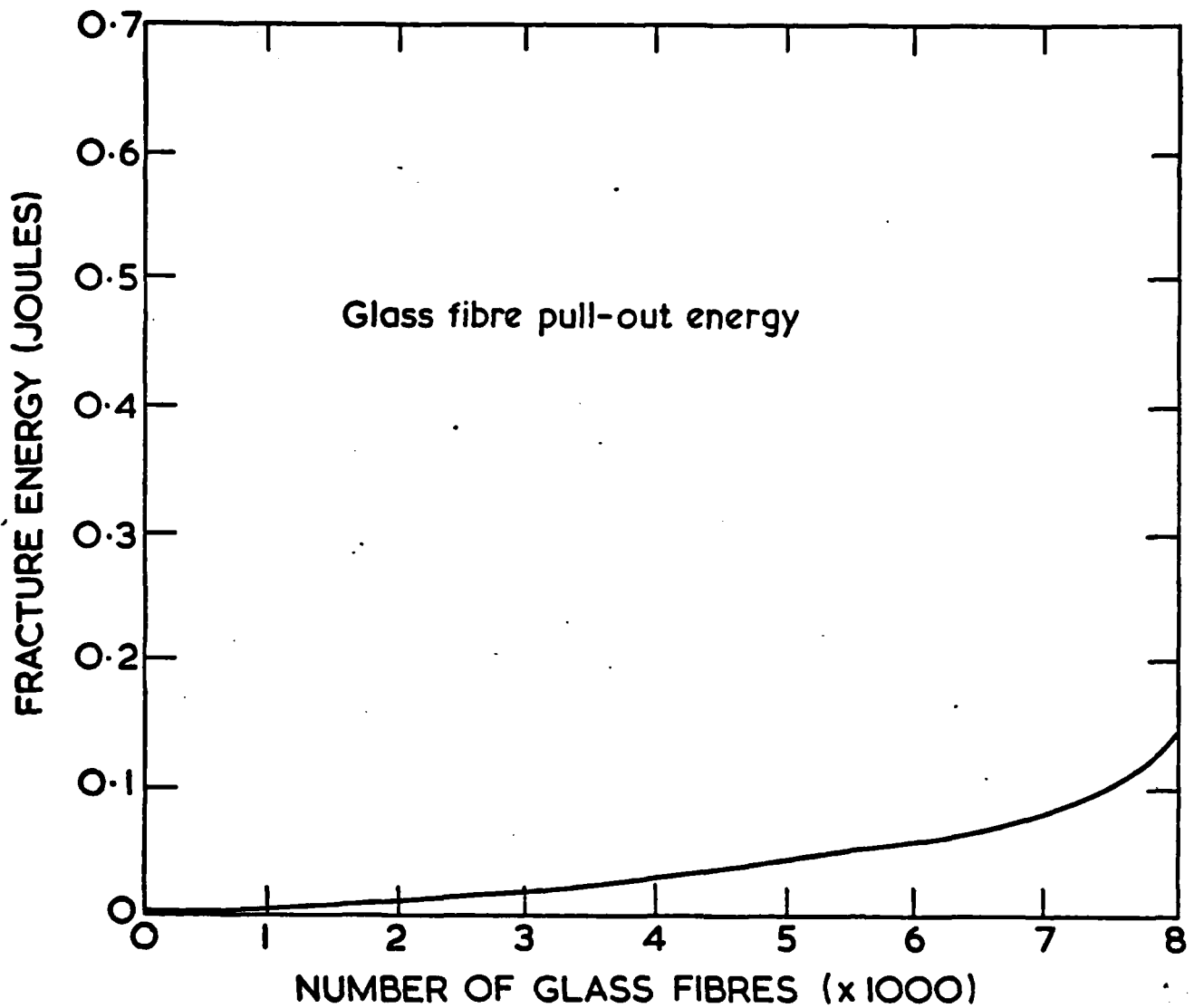


Fig. 20 An estimation of the work done in pulling broken glass fibres out of their epoxy matrix sockets, based on data of fibre pull-out length, together with eqn. (13).

FRACTURE ENERGY (Joules)

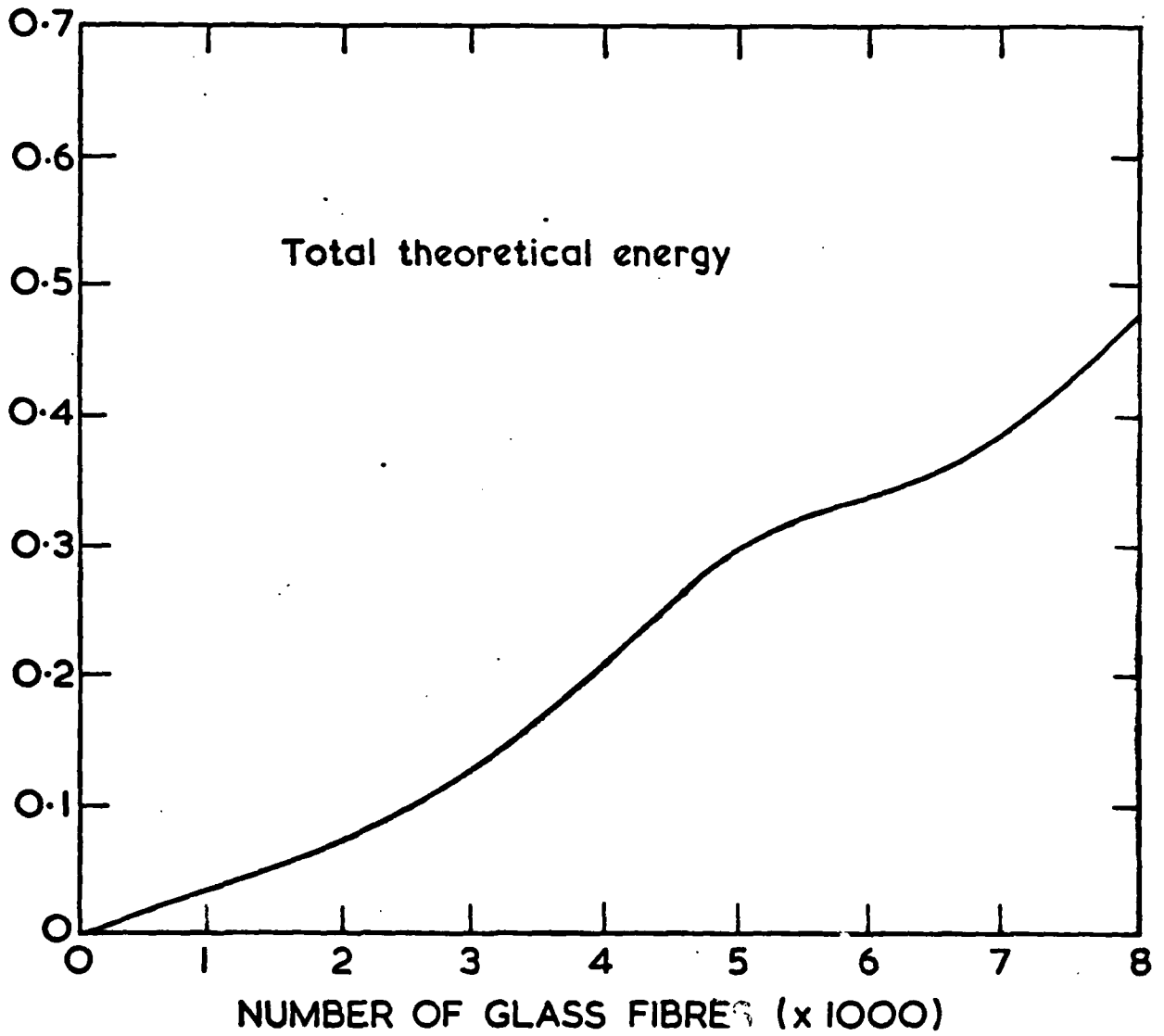


Fig. 21 Total theoretical fracture energy of glass fibres in epoxy determined by combining data of fibre debond length and fibre pull-out length with eq. (14).

FRACTURE ENERGY (JOULES)

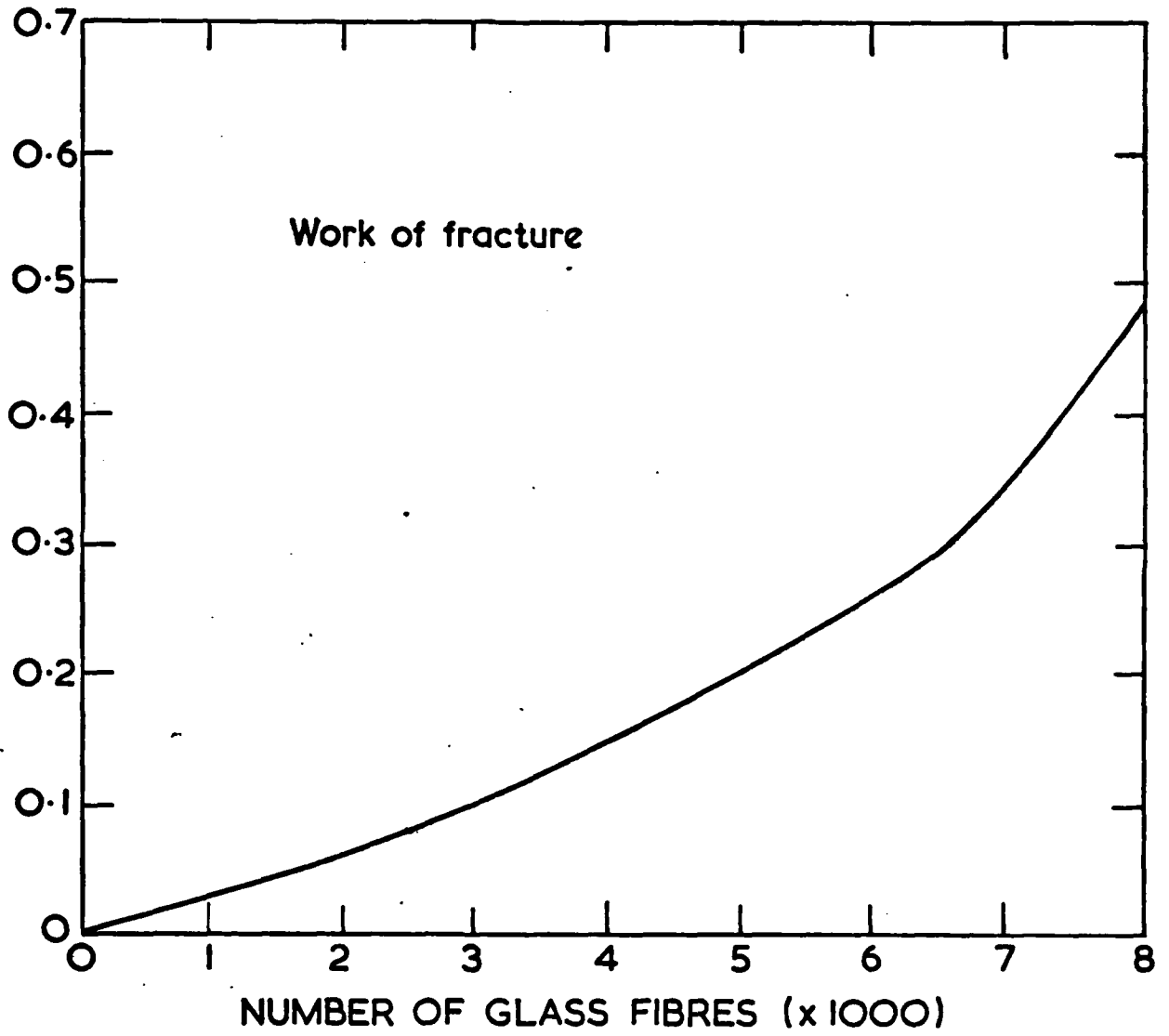


Fig. 22 Experimental work of fracture for glass fibres in epoxy.

FRACTURE ENERGY (kJ/m²)

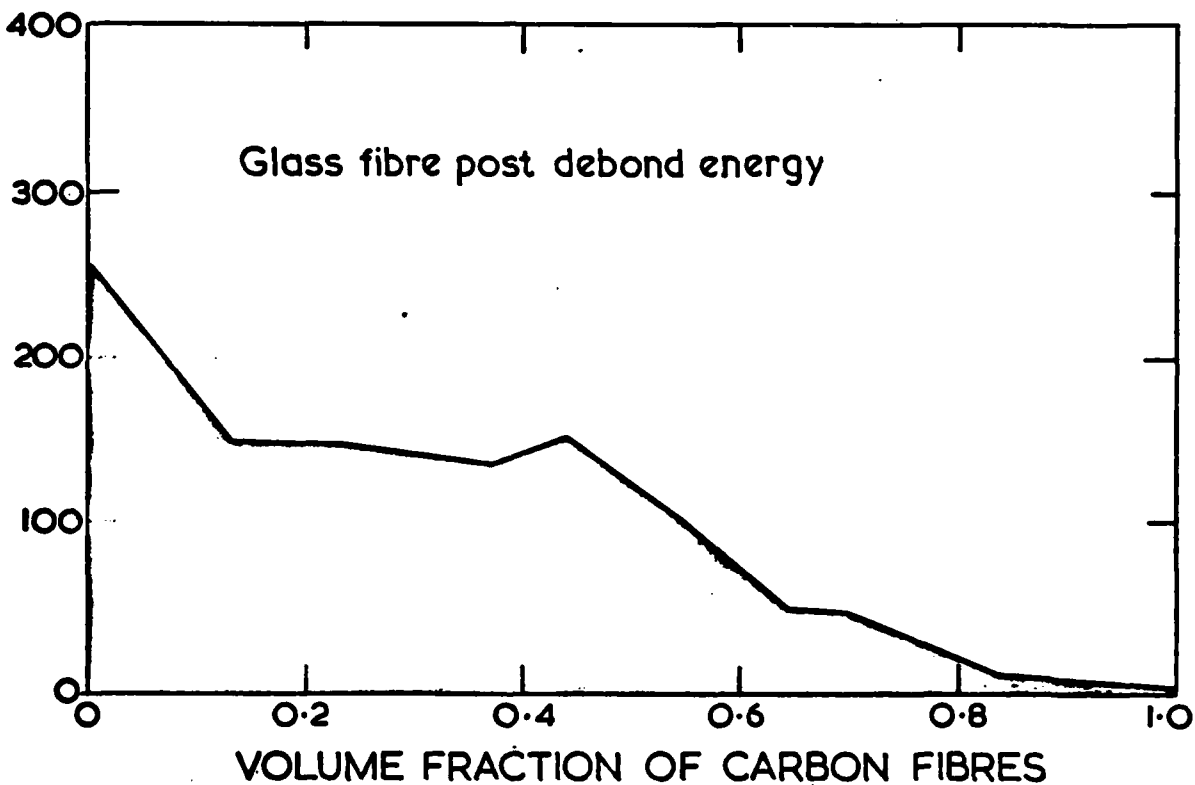


Fig. 23 An estimation of the energy dissipated when a glass fibre debonds and slides in its matrix socket in a hybrid composite system (epoxy matrix).

FRACTURE ENERGY (kJ/m²)

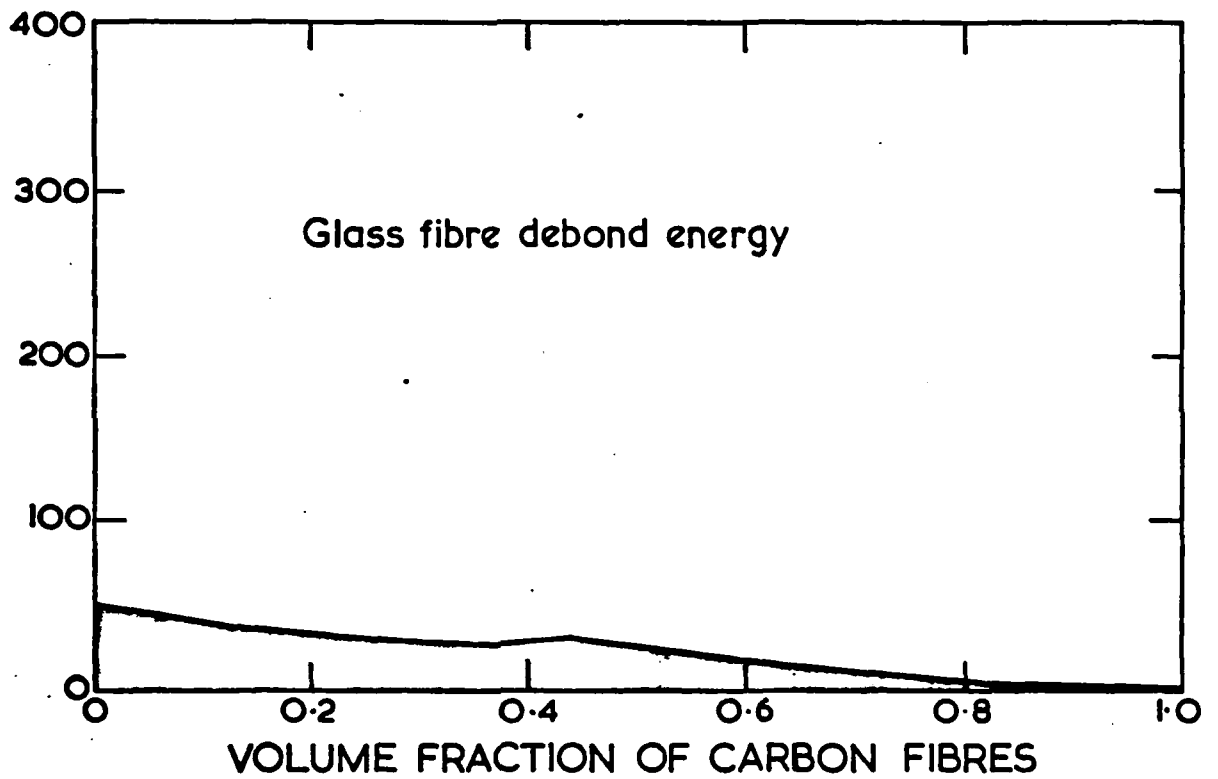


Fig. 24 An estimation of the release of stored elastic strain energy when a debonded glass fibre snaps in a hybrid composite system (epoxy matrix).

FRACTURE ENERGY (kJ/m^2)

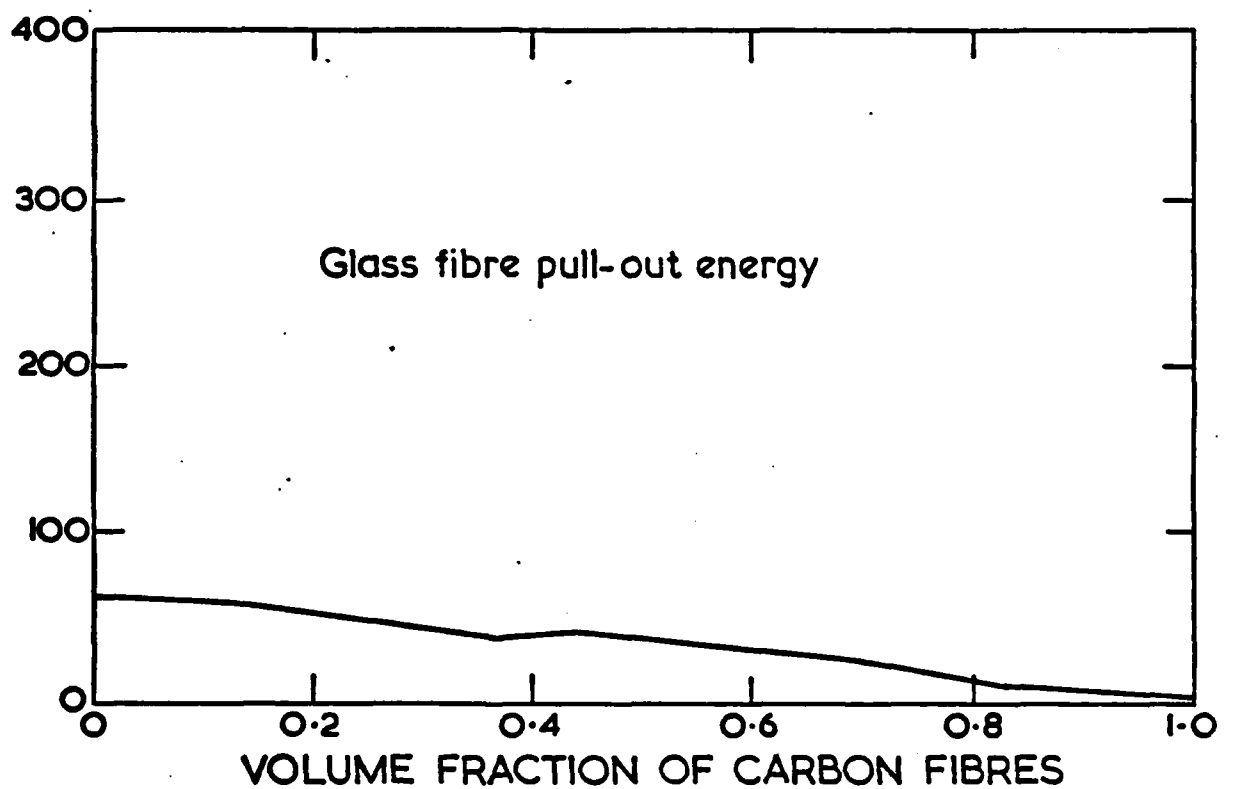


Fig. 25 An estimation of the work done in pulling a broken glass fiber out of a cracked matrix in a hybrid composite system (epoxy matrix).

FRACTURE ENERGY (kJ/m²)

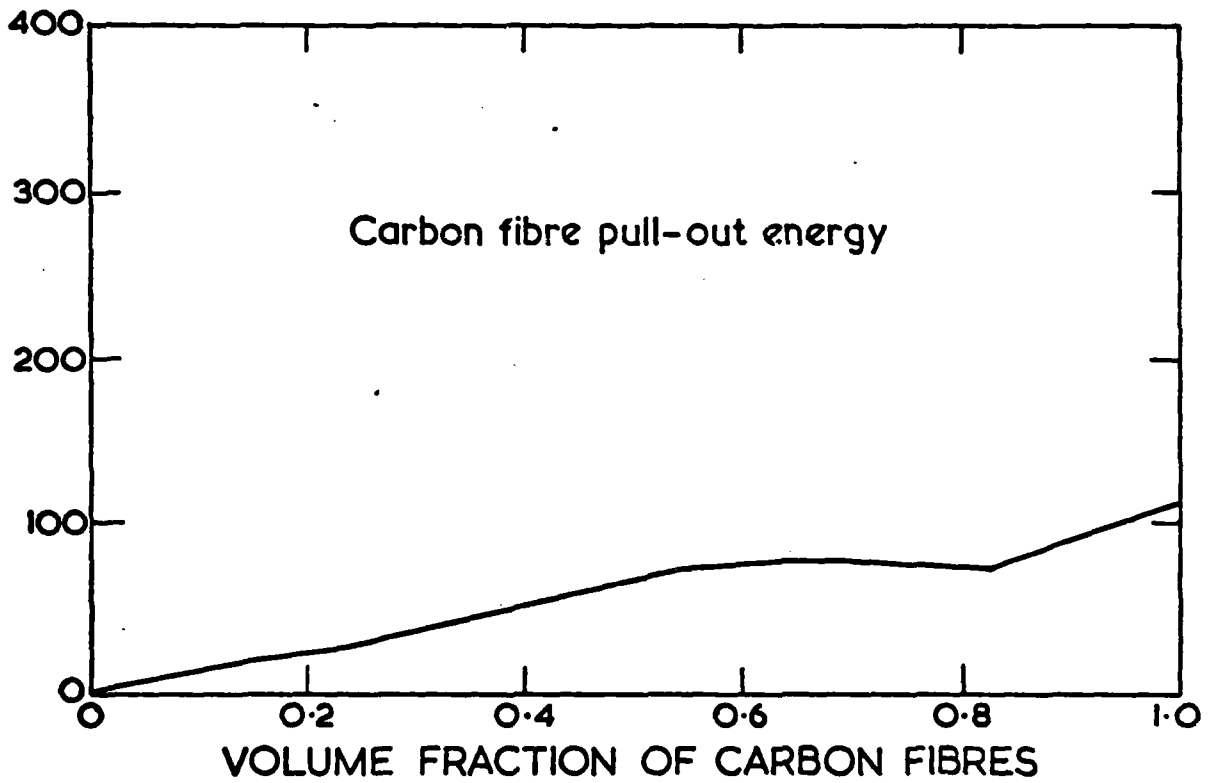


Fig. 26 An estimation of the work done in pulling a broken carbon fibre out of a cracked matrix in a hybrid composite system (epoxy matrix).

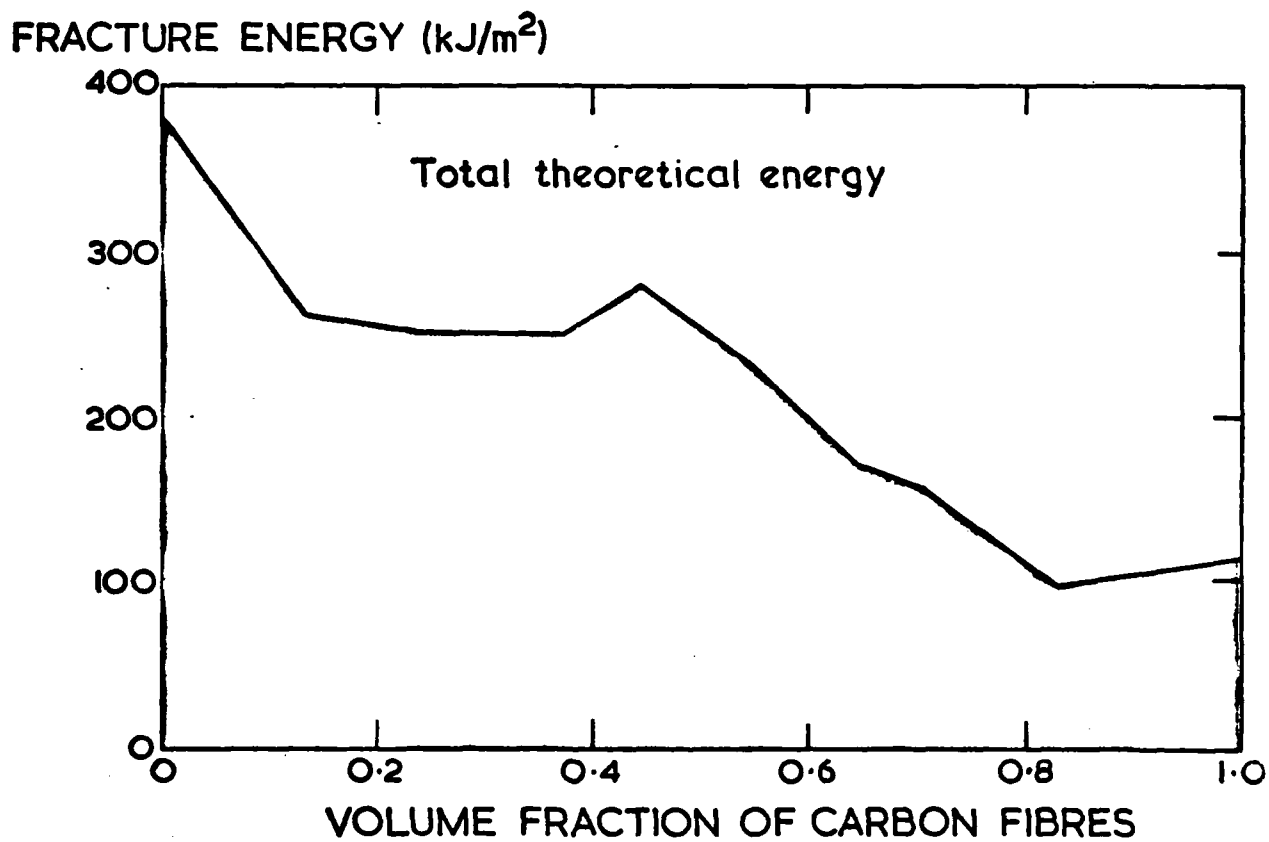


Fig. 27 Total theoretical fracture energy of a hybrid composite system determined from data of debonded length and pull-out length of glass fibers and carbon fibers in epoxy.

FRACTURE ENERGY (kJ/m²)

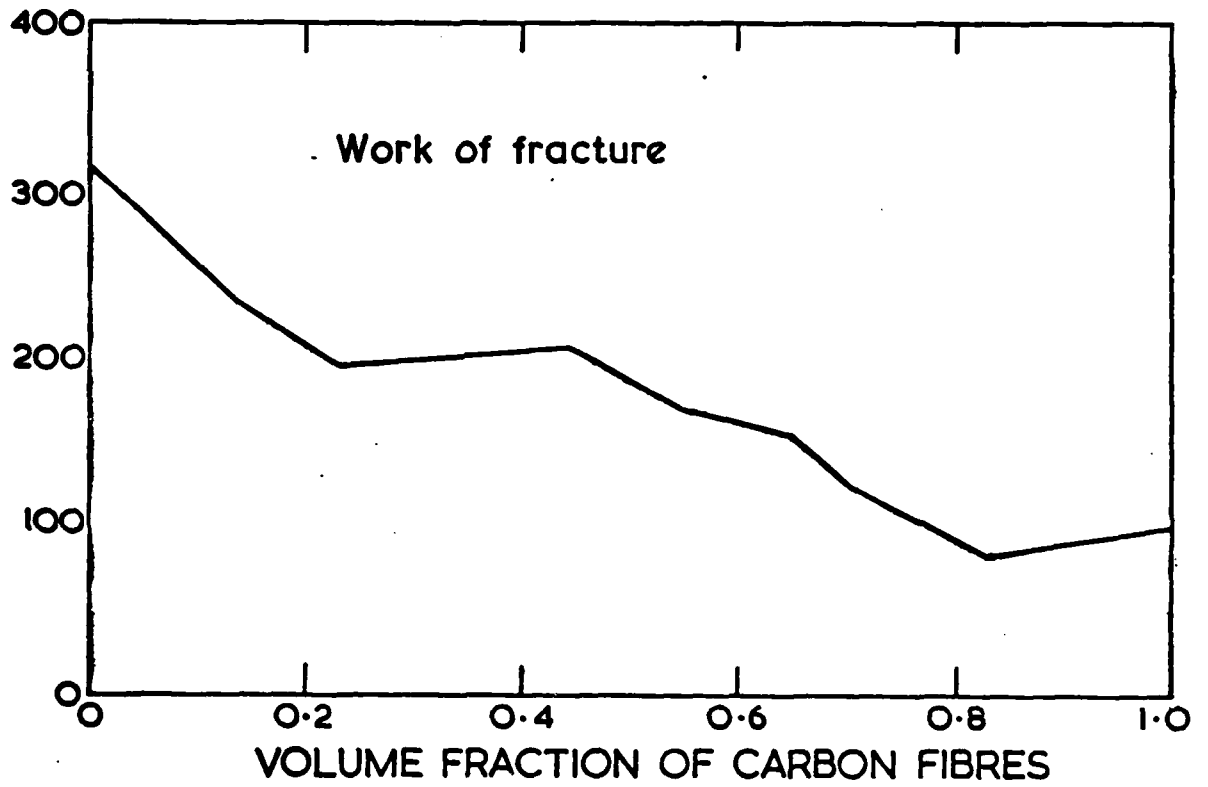


Fig. 28 Experimental work of fracture of a hybrid composite system (glass fibres and carbon fibres in epoxy).

GLASS FIBER
POST DEBOND SLIDING ENERGY (KJ/m²)

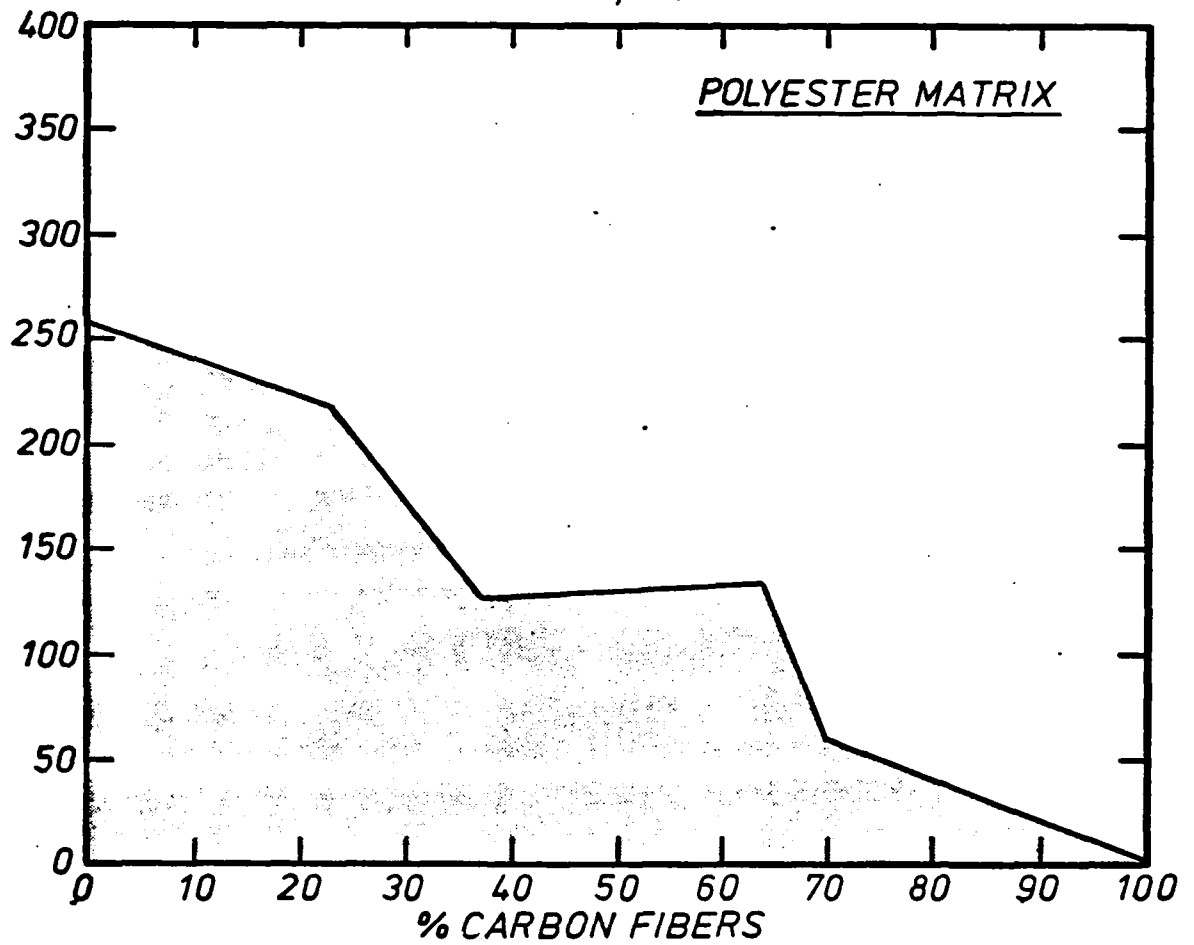


Fig. 29 Estimation of the energy dissipated when a glass fibre debonds and slides in its matrix socket in a hybrid composite system (polyester matrix).

GLASS FIBER DEBONDING ENERGY (KJ/m²)

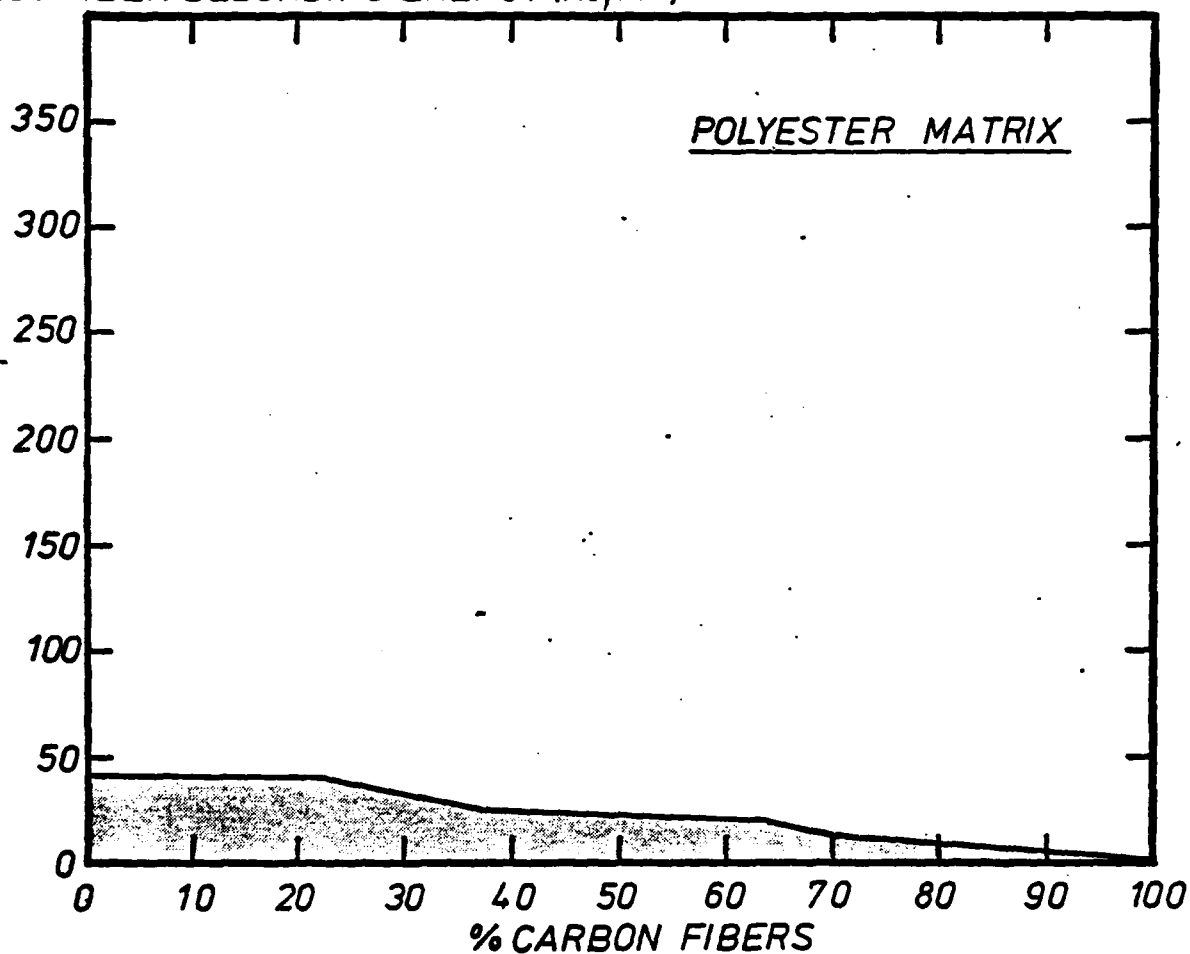


Fig. 30 Estimation of the release of stored elastic strain energy when a debonded glass fibre snaps in a hybrid composite system (polyester matrix).

GLASS FIBER PULL OUT ENERGY (KJ/m²)

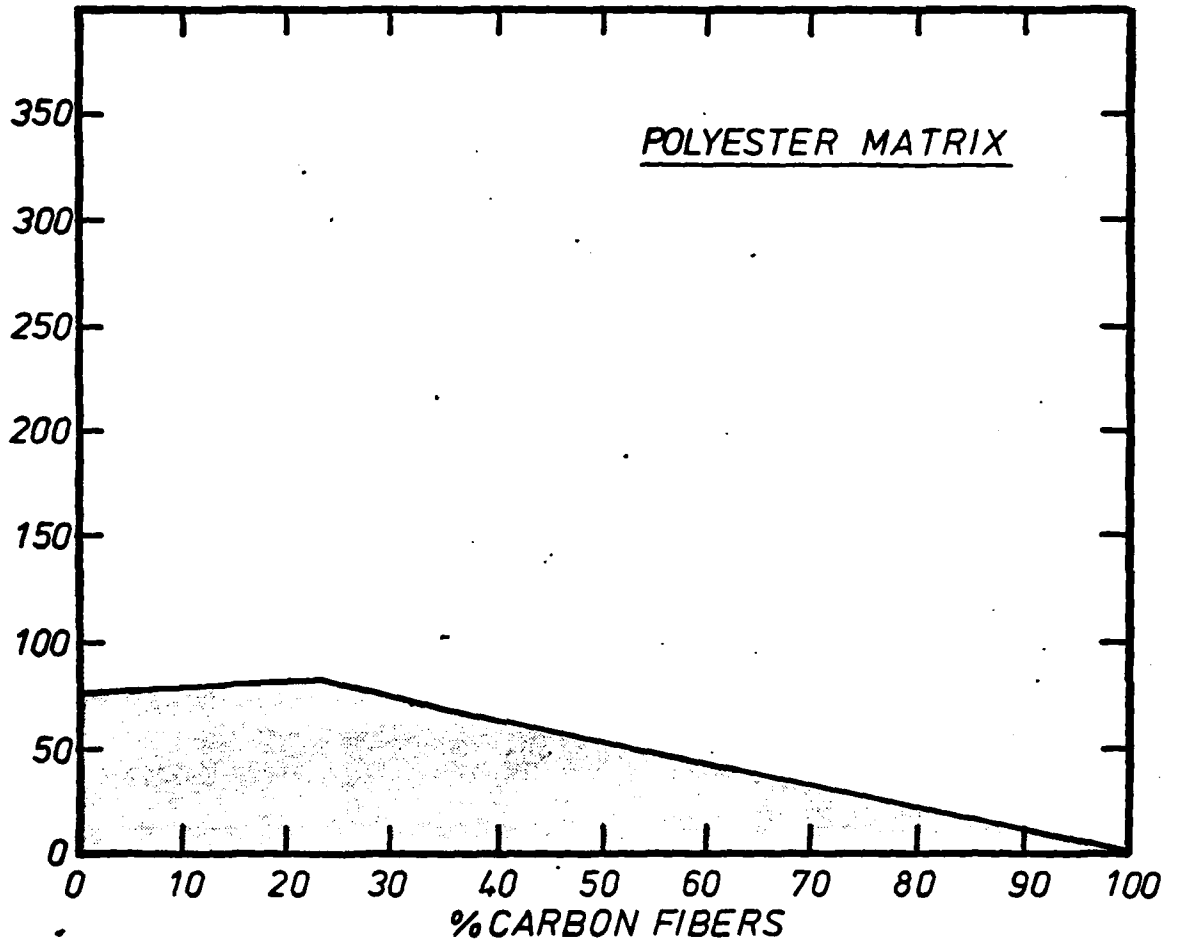


Fig. 31 Estimation of the work done in pulling a broken glass fibre out of its matrix socket in a hybrid composite system (polyester matrix).

CARBON FIBER PULL OUT ENERGY (KJ/m²)

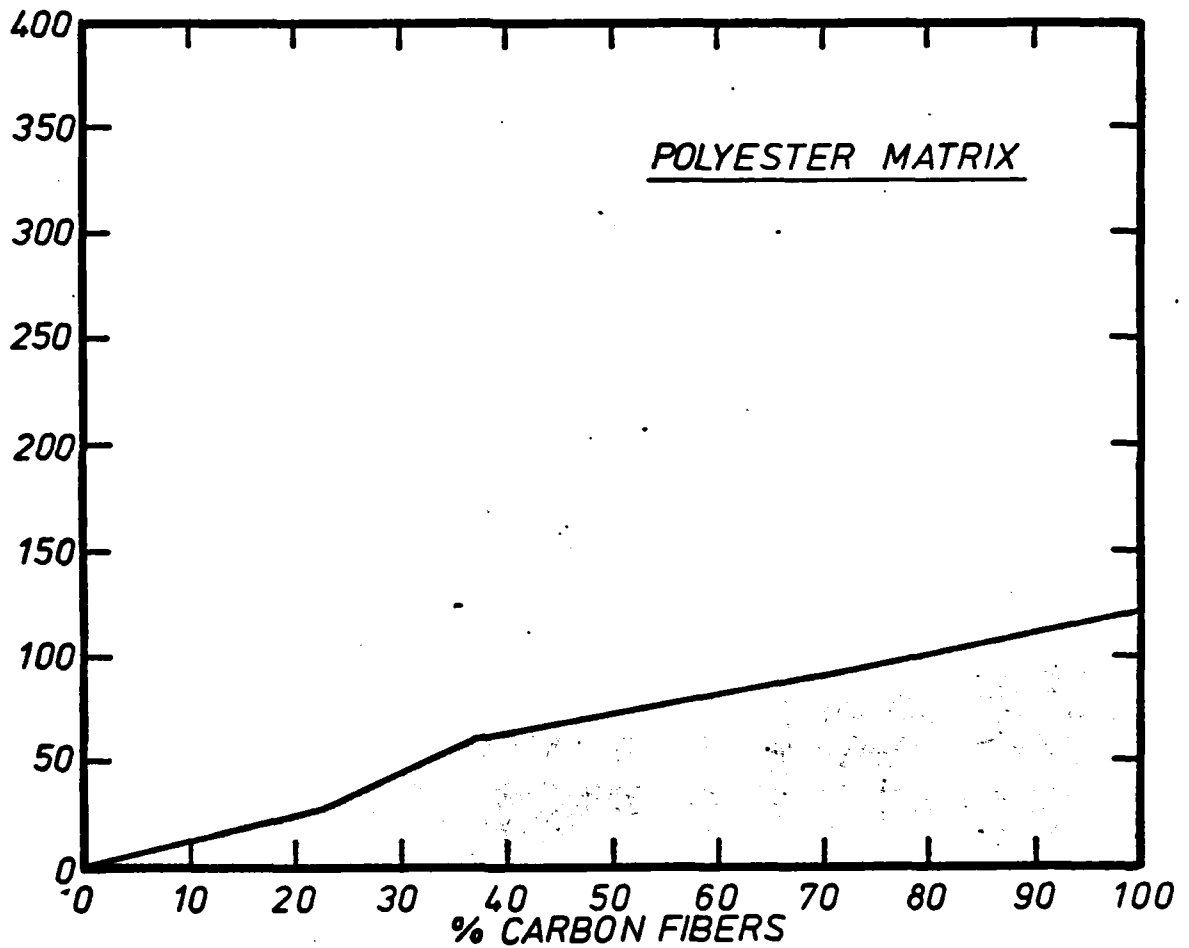


Fig. 32

Estimation of the work done in pulling a broken carbon fibre out of its matrix socket in a hybrid composite system (polyester matrix).

TOTAL FRACTURE ENERGY (KJ/m²)

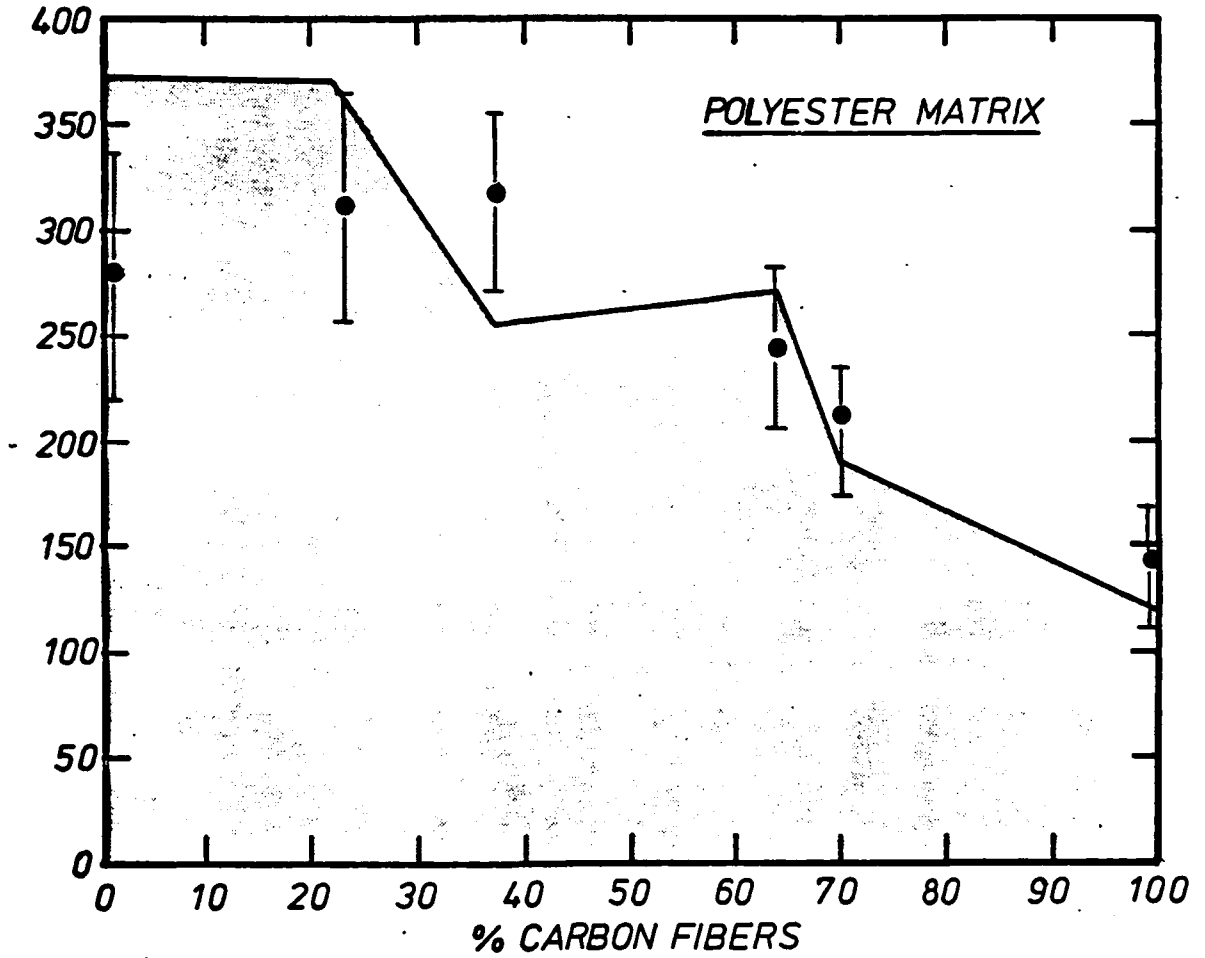


Fig. 33 Total theoretical fracture energy of a hybrid composite system (carbon and glass fibres in polyester). The points represent measured work of fracture data.

WORK OF FRACTURE

KJ/m²

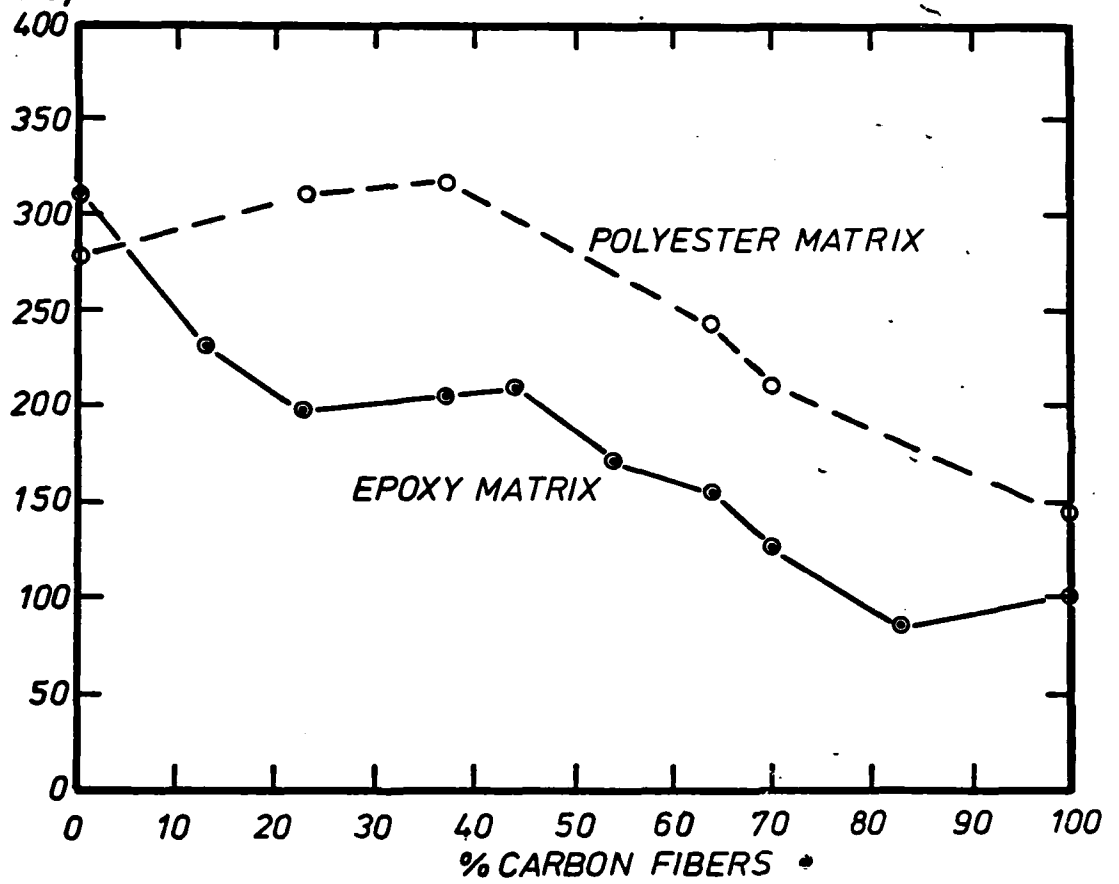


Fig. 34 Comparison between experimental work of fracture data of polyester and epoxy hybrid composite systems.

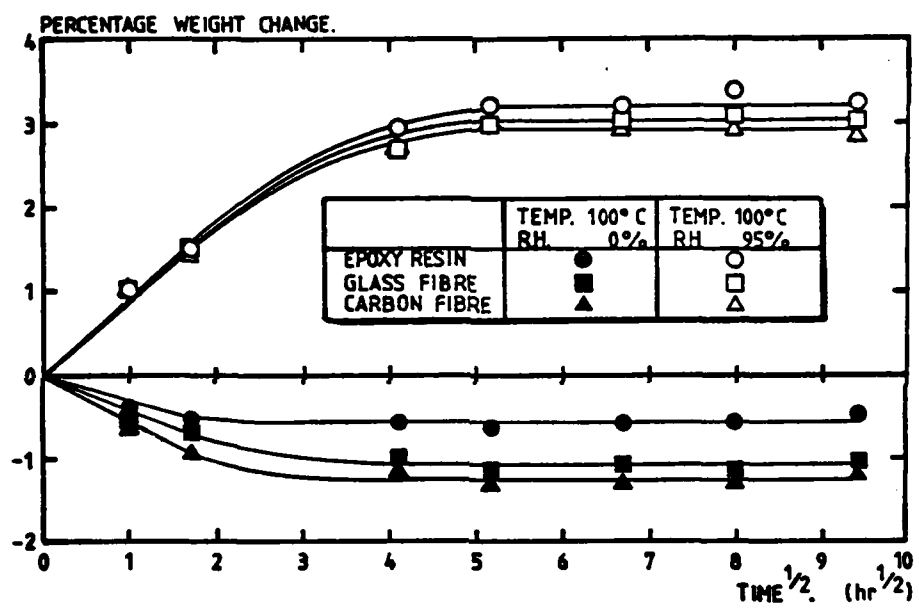


Fig. 35 Change of weight of resin and composite as a function of humidity and aging time.

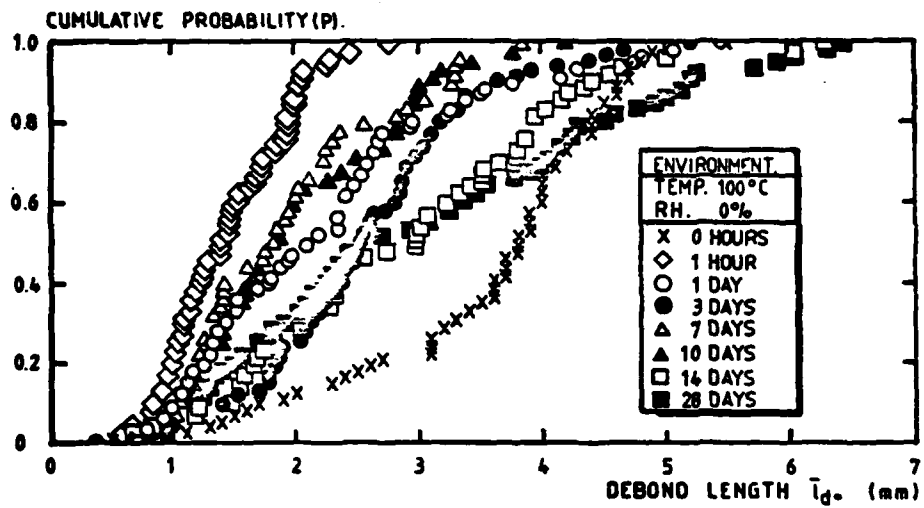


Fig. 36 Distribution of glass fibre debond lengths for various aging times (100 °C, 0 % RH).

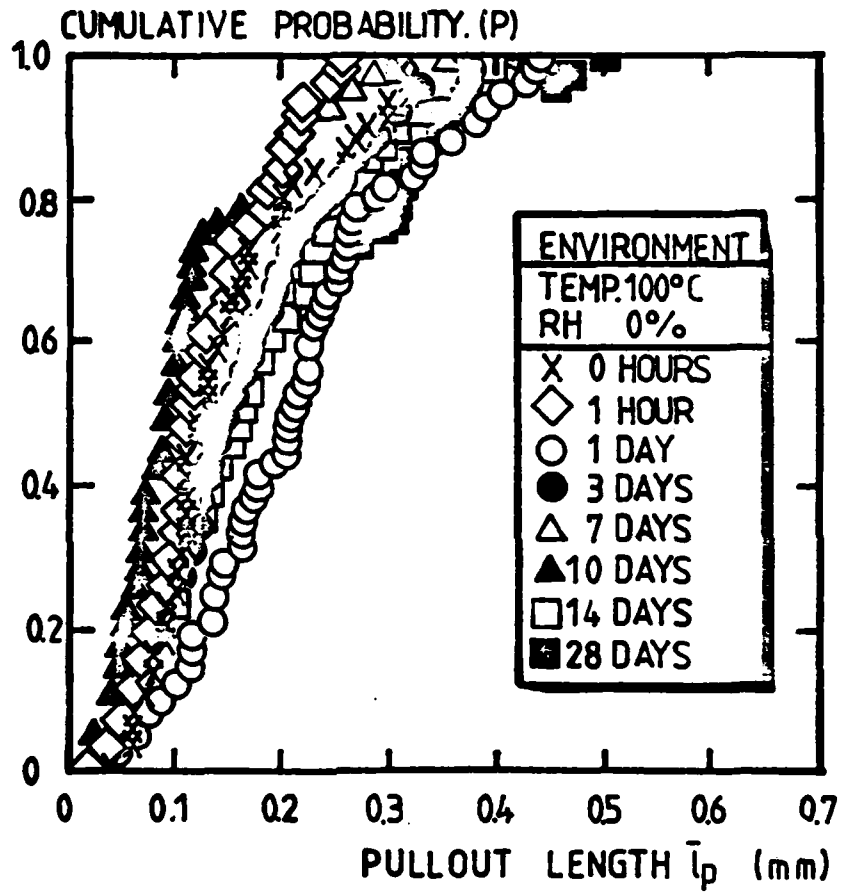


Fig. 37 Distribution of glass fibre pull-out lengths for various aging times (100 °C, 0 % RH).

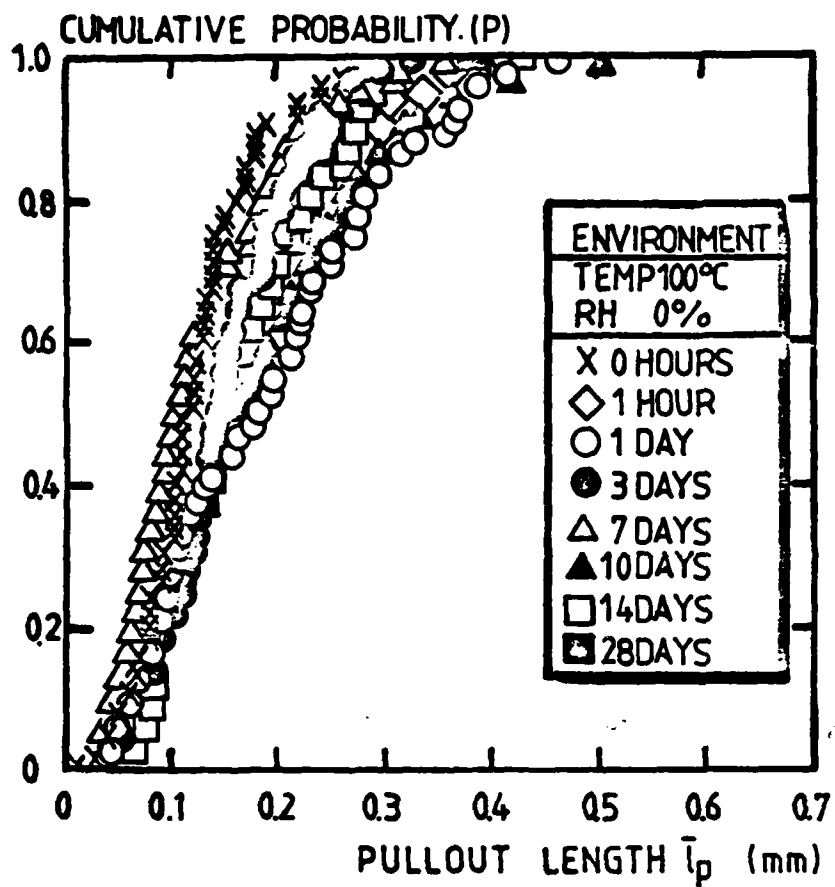


Fig. 38 Distribution of carbon fibre pull-out lengths for various aging times (100 °C, 0 % RH).

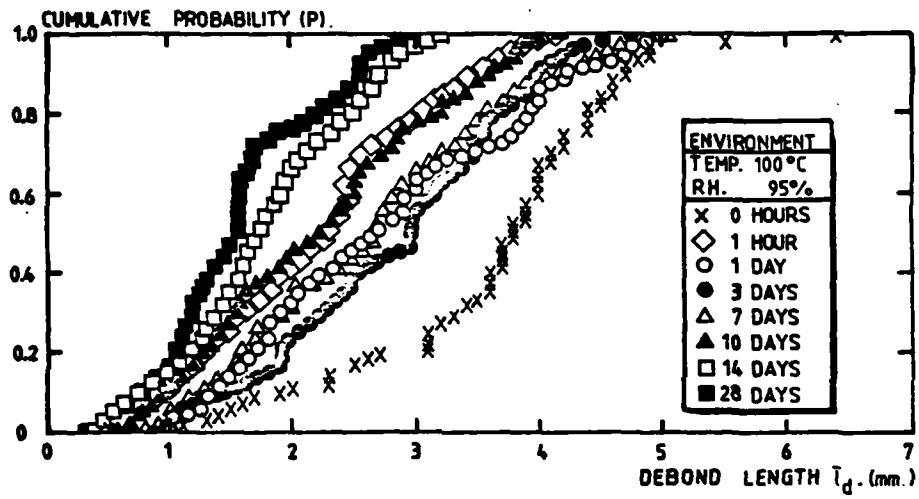


Fig. 39 Distribution of glass fibre debond lengths for various aging times (100 °C, 95 % RH).

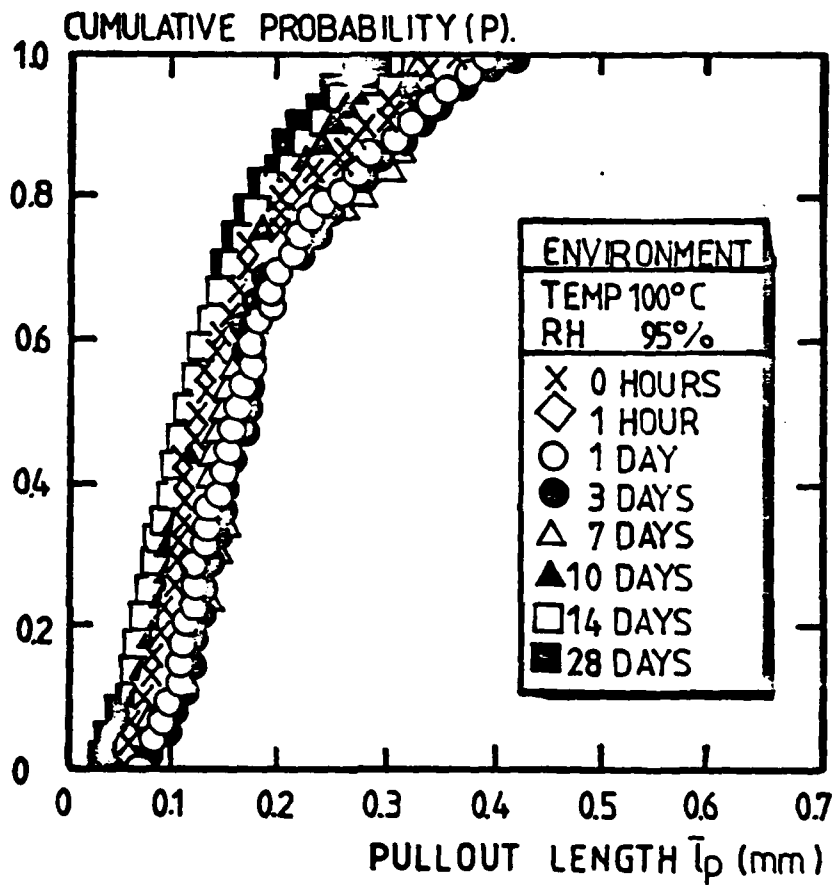


Fig. 40 Distribution of glass fibre pull-out lengths for various aging times (100 °C, 95 % RH).

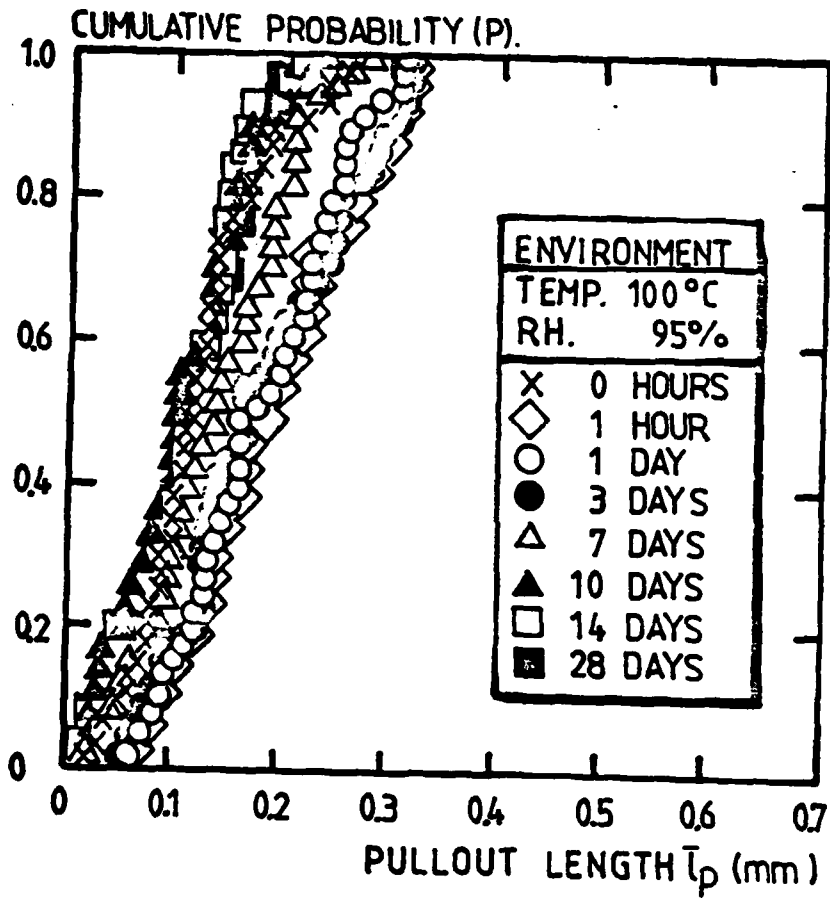


Fig. 41 Distribution of carbon fibre pull-out lengths for various aging times (100 °C, 95 % RH).

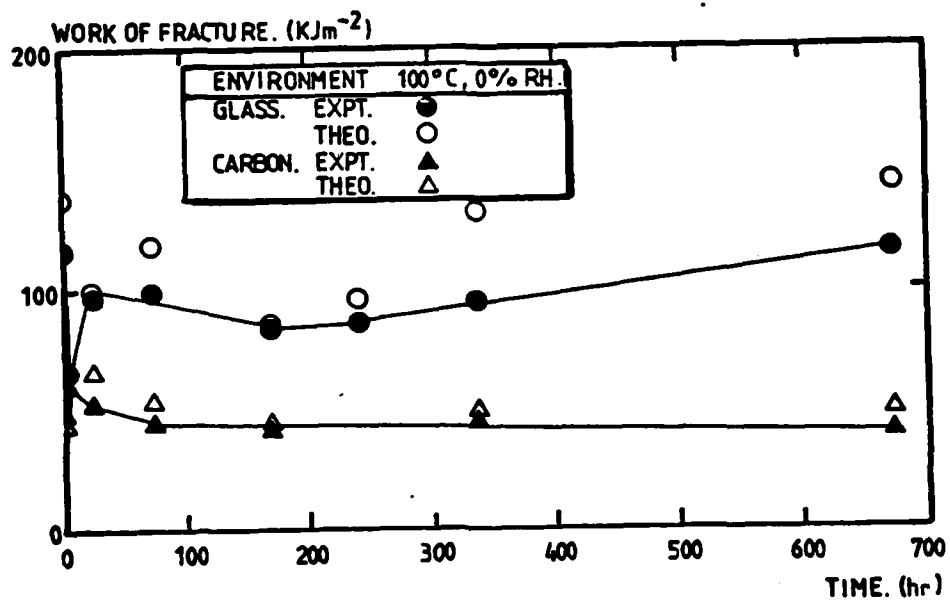


Fig. 42 — Work of fracture of composite as a function of aging time (100 °C, 0 % RH).

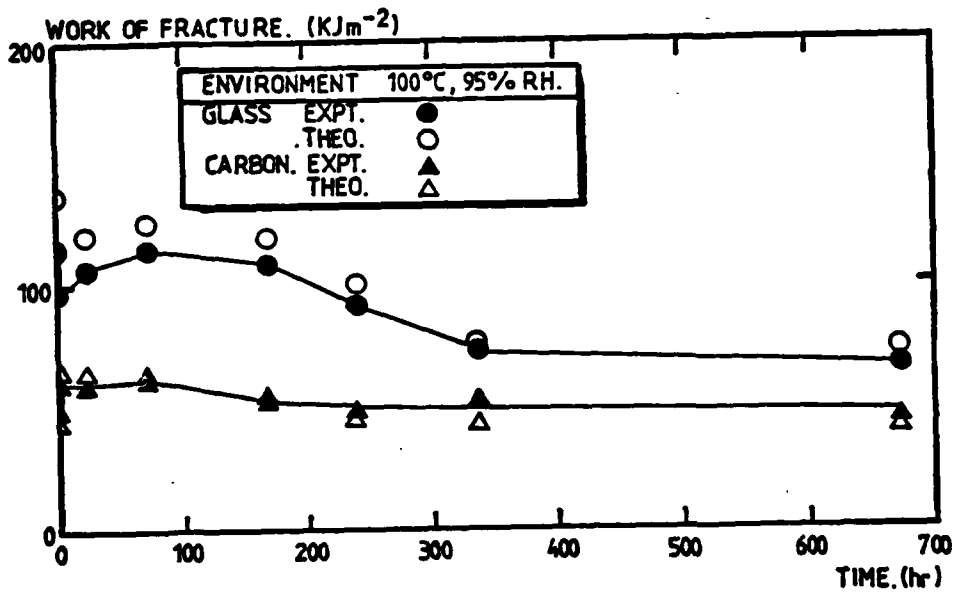


Fig. 43 Work of fracture of composite as a function of aging time. (100 °C, 95 % RH)

